Study of compliant mechanisms and flexible hinges in topology optimization

Document:

Report

Author:

Marina Masip Freixinet

Director/Co-director:

Alex Ferrer Ferre
Jose Antonio Torres Lerma

Degree:

Bachelor in aerospace vehicles engineering

Examination session:

Spring

BACHELOR FINAL THESIS

Declaration of honor

I declare that,

- The work and effort dedicated to this Bachelor's Thesis is completely my work.

- All references from other people's work have been clearly cited.

Finally, I understand that a violation of this statement leaves me subject to disciplinary action, provided by the Universitat Politècnica de Catalunya - BarcelonaTECH.

Marina Masip Freixinet

Abstract

This thesis presents a comprehensive study on the application of compliant mechanisms and flexible hinges in topology optimization. Compliant mechanisms are a promising approach for achieving desired functionalities and structural flexibility in engineering designs. By exploiting the inherent elasticity of materials, compliant mechanisms offer advantages such as reduced complexity, improved reliability, and enhanced performance. Topology optimization, conversely, allows obtaining compliant mechanisms with reduced weight through the creation of holes, thus achieving an optimized design. In this work, we explore the integration of compliant mechanisms and flexible hinges within the framework of topology optimization, aiming to propose a method of improvement for the design efficiency and performance of structures in the aerospace field.

The thesis begins with a thorough literature review of compliant mechanisms and their role in current aerospace applications. Various design principles and analysis techniques are examined to establish a solid foundation for the subsequent chapters. The study then focuses on the implementation of mathematical models and computational algorithms to incorporate compliant mechanisms and flexible hinges into the topology optimization process.

To validate the proposed approach, a series of numerical experiments are conducted. Various case studies are considered, including a gripping and inverter mechanisms. The results demonstrate the effectiveness of compliant mechanisms and flexible hinges in enhancing the performance of optimized structures. The compliant mechanisms exhibit improved flexibility, adaptability, and energy absorption capabilities enabling smooth and controlled motion.

Overall, this thesis significantly contributes to the understanding and implementation of compliant mechanisms and their integration with topology optimization techniques. The study not only showcases their potential for creating innovative and efficient designs across various engineering disciplines but also emphasizes their particular relevance in the aerospace field. By exploring the application of compliant mechanisms and topology optimization in aerospace engineering, it has been seen that this cutting-edge technology is opened up for new avenues for further research and development.

Keywords: Compliant mechanisms, Flexible hinges, Topology optimization, Aerospace engineering, Design efficiency, Computational algorithms.

Resumen

Esta tesis presenta un estudio exhaustivo sobre la aplicación de mecanismos flexibles y bisagras en la optimización topológica. Los mecanismos flexibles son un enfoque prometedor para lograr funcionalidades deseadas y flexibilidad estructural en diseños de ingeniería. Al aprovechar la elasticidad inherente de los materiales, los mecanismos flexibles ofrecen ventajas como una menor complejidad, una mayor confiabilidad y un rendimiento mejorado. Por su parte, la optimización topológica permite obtener mecanismos conformes con un peso reducido a través de la creación de agujeros, logrando así un diseño optimizado. En este trabajo, exploramos la integración de mecanismos flexibles y bisagras dentro del marco de la optimización topológica, con el objetivo de proponer un método para mejorar la eficiencia y el rendimiento del diseño de estructuras en el campo aeroespacial.

La tesis comienza con una exhaustiva revisión bibliográfica de los mecanismos flexibles y su papel en las aplicaciones aeroespaciales actuales. Se examinan varios principios de diseño y técnicas de análisis para establecer una base sólida para los capítulos posteriores. El estudio se centra luego en la implementación de modelos matemáticos y algoritmos computacionales para incorporar mecanismos flexibles y bisagras dentro del proceso de optimización topológica.

Para validar el enfoque propuesto, se llevan a cabo una serie de experimentos numéricos. Se consideran diversos estudios de casos, incluyendo mecanismos de agarre e inversores. Los resultados demuestran la eficacia de los mecanismos flexibles y las bisagras en la mejora del rendimiento de las estructuras optimizadas. Los mecanismos flexibles exhiben una flexibilidad, adaptabilidad y capacidad de absorción de energía mejoradas, lo que permite un movimiento suave y controlado.

En general, esta tesis contribuye significativamente a la comprensión e implementación de mecanismos flexibles y su integración con técnicas de optimización topológica. El estudio no solo muestra su potencial para crear diseños innovadores y eficientes en diversas disciplinas de ingeniería, sino que también destaca su relevancia particular en el campo aeroespacial. Al explorar la aplicación de mecanismos flexibles y optimización topológica en la ingeniería aeroespacial, se ha visto que esta tecnología de vanguardia se abre a nuevas oportunidades para futuras investigaciones y desarrollos.

Palabras clave: Mecanismos flexibles, Bisagras flexibles, Optimización topológica, Ingeniería aeroespacial, Eficiencia de diseño, Algoritmos computacionales.

Contents

List of Figures

List of Tables

List of abbreviations

CMs: Compliant mechanisms

OOP: Object-Oriented Programming

FEM: Finite Elements Method

TO: Topology Optimization

ESA: European Space Agency

NASA: National Aeronautics and Space Administration

AIAA: American Institute of Aeronautics and Astronautics

VGT: Variable Geometry Truss

PDE : Partial differential equation

SIMP: Isotropic Material with Penalization

KKT: Karush–Kuhn–Tucker

CSA: Civil, Structural and Architectural

MEMS: Micro Electro-Mechanical Systems

NEMS: Nano Electro-Mechanical Systems

AIS: Automatic Identification System

AFRL: Air Force Research Laboratory

GMA: Giant Magnetostrictive Actuator

LET: Lamina Emergent Torsional

MIS: Minimally Invasive Surgery

AM: Additive Manufacturing

MMA: Method of Moving Asymptotes

MS: Motion Stage

FTEFs: Flexible Trailing Edge Flaps

EU: European Union

EASA: European Aviation Safety Agency

SDGs : Sustainable Development Goals

Chapter 1

Introduction

1.1 Object

The objective of this bachelor's thesis is to conduct an extensive literature review on Compliant Mechanisms (CMs) and provide an in-depth study of the fundamental concepts of topology optimization for the purpose of applying them to the numerical design of a compliant mechanism within a given initial design domain. To better comprehend the codes utilized in topology optimization studies, a course on clean code development and Object-Oriented Programming (OOP) has been undertaken. The thesis will present a comprehensive and meticulous overview of the current state of the art, offering detailed explanations of the principal mechanisms involved. Additionally, a comprehensive background in topology optimization will be explored to acquire a broad understanding of this field. Subsequently, a topology optimization process will be employed to design a compliant mechanism that, if feasible, will be fabricated using additive manufacturing technologies.

1.2 Scope

This study focuses on a thorough understanding of the operation of compliant mechanisms encompassing the following states:

- A clean code development practice will be done in order to be able to understand the codes used in topology optimization including the use of Object-Oriented Programming in the Swan repository from Git Hub environment.

- A meticulous analysis of the most significant mechanisms and the latest literature in the field will be conducted.

- A comprehensive review of the utilization of Finite Element Method (FEM) in the context of elastic problems will be conducted.

- A study of topology optimization will be performed to understand the basics of this area and apply the knowledge to CMs.

- As a final objective, a numerical design of CMs based on some of the mechanisms analysed in the first part of the study will be done following the next steps:

  - Case studies definition: Gripper and inverter mechanisms.

  - Simulations set-up

  - Analysis of results

- Finally, if possible, the mechanism will be printed using additive manufacturing technology.

- A possible application of CMs inside the aerospace field will be provided.

- Project time management.

Although the main focus of this study is on topology optimization of CMs, it is not feasible to develop a code entirely from within the allotted time frame. Nonetheless, a comprehensive understanding of the existing code will be achieved as part of this research, along with the preparation of input deck files with tunning parameters.

1.3 Requirements

In order to fully complete the project, certain specifications need to be met. The primary requirement for the final stage of the design involves access to a 3D printer for fabricating the project's ultimate design. However, it should be noted that while this aspect is not integral to the study, its non-fulfillment will not compromise the principal objective, which is to gain a comprehensive understanding of CMs.

Furthermore, it is essential to emphasize the study's robust theoretical foundation, necessitating access to a reliable database to obtain articles on CMs. This can be accomplished through institutional authentication. Additionally, it is important to ensure that the design domain and boundary conditions cited in the literature are capable of replicating a CM during the topology optimization simulations. Lastly, access to a MATLAB license is also indispensable, which can once again be acquired through institutional channels.

1.4 Justification

Compliant mechanisms are single-piece flexible structures, which use elastic deformation to achieve force and motion transmission and accomplish their function due to the deformation of one or more slender segments of their members [1, 2]. These mechanisms represent a burgeoning area of research that is gaining prominence in the aerospace domain. Over the past decade, this novel class of mechanisms has garnered significant attention from scientists due to its compelling advantages and potential to address the shortcomings associated with conventional mechanisms, particularly in aerospace applications. These challenges encompass issues such as lubrication outgassing, friction and binding of joints, and inadequate force or torque safety margins, which necessitate special considerations for mechanisms operating in space to mitigate the risk of failure.

Furthermore, the study places emphasis on topology optimization, as it represents a valuable approach to achieving weight reduction in structures while optimizing some properties, such as maximum stiffness or maximum output displacements. The pursuit of lightweight structures holds significant relevance in the aerospace industry, as it directly contributes to the goal of minimizing fuel consumption and mitigating environmental impact.

On the other hand, the interest in additive manufacturing stems from the fact that it is an emerging technology that makes it possible to design almost any structure, even if the shape is complex or with unintuitive holes, and is also cheaper than other manufacturing processes.

Many studies have yet to be conducted, but promising results have been obtained and some space agencies and researchers are showing interest in investing and investigating in this area. Combining these three areas of the engineering cloud yields an interesting result that solves some current problems and provides a new way to understand structures and mechanisms.

In particular, ESA is conducting important research in this area and doing a significant investment. In fact, a call for a founding project form ESA (Additive Manufactured compliant mechanism system with integrated sensor/actuator) is the main inspiration for this study.

Chapter 2

State-of-the-art Compliant Mechanisms

This chapter presents a comprehensive investigation into the existing body of knowledge concerning compliant mechanisms, encompassing their applications, particularly in the filed of space applications, and elucidating the advantages offered by these mechanisms.

2.1 Compliant mechanisms

Nature provides an example of how to effectively create controlled motion. Most moving components in nature are flexible instead of stiff, and the motion comes from bending the flexible parts instead of rigid parts connected with hinges (for example, consider hearts, elephant trunks, and bee wings). The smaller the specimen, the more likely it is to use the deflection of flexible components to obtain its motion [3].

Compliant mechanisms are single-piece flexible structures, which use elastic deformation to achieve force and motion transmission and accomplish their function due to the deformation of one or more slender segments of their members [1, 2]. CMs gain some or all of its motion from the relative flexibility of its members rather than from rigid body joints alone. Such mechanisms, with built-in flexible segments, are simpler and replace multiple rigid parts, pin joints and add-on springs [1].

Due to their monolithic nature, CMs possess two main benefits over conventional rigid-link mechanisms, namely no relative motion among pieces and no overlapping pieces. The absence of relative motion implies the absence of sliding friction, which eliminates wear, noise, vibration and the need for lubrication. Consequently, less maintenance is required. The fact that there are no overlapping pieces allows fewer parts and single piece production, which reduces the assembly and weight. Therefore, compactness, miniaturization are enhanced while production costs are reduced [2].

All these benefits help to create more innovative designs and actuation arrangements which increase the solution search space [2].

2.2 Current challenges

It has been unequivocally ascertained that CM exhibit numerous advantages in comparison to rigid body joint mechanisms. Nonetheless, it is imperative to acknowledge that certain significant challenges persist in this field, necessitating further research and resolution.

One drawback of CMs is that most are unable to undergo continuous rotation. Also, if a fully compliant mechanism is constructed from a single layer of material, then special care has to be taken to ensure that moving segments of the compliant mechanism do not collide with other segments of the same mechanism [3].

The performance of CMs is highly dependent on the material properties, which are not always well known. Moreover, the deflections experienced by this mechanisms often extend beyond the range of linearized beam equations and this can make their analysis and design more complicated [3].

Furthermore, because most compliant mechanisms undergo repeated loading, it is important to consider the fatigue life of the device. An understanding of how to achieve controlled compliant mechanism motion and the associated stresses, makes it possible to design compliant mechanisms with the desired fatigue life. Factors such as stress concentrations, the operating temperature, and other environment conditions can affect the fatigue life [3].

Henceforth, it becomes apparent that the design of CMs encompasses numerous challenges arising from existing issues such as the integration of functions into fewer components, nonlinear displacements, dependence on material properties, the need to avoid self collisions during motion, and designing for appropriate fatigue life, all combine to make the design of compliant mechanisms nontrivial and often difficult [3].

2.2.1 Space mechanisms challenges

Satellites, rovers, the international space station, and other space vehicles require mechanisms to perform mechanical tasks. These space mechanisms have been designed to perform in the demanding environments of space and launch [4].

Current space mechanisms are almost entirely composed of traditional rigid-link assemblies. However, the harsh environments of space impose demanding requirements and rigid-link mechanisms can experience a variety of issues, including lubrication outgassing, friction and binding of joints, and inadequate force or torque margin of safety. The mission objectives or desired mechanism functionality also have demanding requirements and rigid-link mechanisms are naturally prone to issues concerning size, weight, and accuracy of motion [4].

Since mechanisms often perform functions that are singularly vital for mission success, a failure could be catastrophic to the mission. Many of the failures of space mechanisms have been documented [5, 6] and occur because of the design trade-offs and inherent challenges [4].

The application of CMs technology could prove vital in overcoming some of the difficult challenges that current space mechanisms face when put in the space environment. Table 2.1 shows key challenges of space mechanisms and which advantages of CMs could possibly address each challenge [4].

Table 2.1: Current space mechanism challenges and the advantages of compliant space mechanisms that overcome those challenges. Extracted from [4].

Challenges of Current Space Mechanism	Advantages of Compliant Space Mechanisms
outgassing of lubrication, friction, wear and binding of joints	elimination of joints requiring lubrication or friction
large mass/weight (and accompanying cost)	significant part count reduction; miniaturization possible
large size/volume	significant part count reduction, increased number of possible joints and design configurations, integration of multiple functions into one mechanism, simpler geometries can lead to a reduction in material and assemblies needed to achieve the required motion
incorrect mechanism stiffness (components assumed rigid are not entirely rigid)	ability to accurately model and predict joint and mechanism stiffnesses; distributed compliance is more accurate for analysis than lumped compliance and it can be accurately calculated
complex or costly to manufacture and integrate	less expensive manufacturing methods possible (e.g. planar); simpler, more integrated geometries can achieve the required motion; significant part count reduction; little or no assembly required
feedback noise in attitude control system due to mechanism dynamics	precision motion provides increased predictability and control over mechanism mode shapes, natural frequencies, and component stiffnesses; can improve isolation from deployment dynamics with distributed compliance
single point failure modes	redundancy in actuation and motion possible; elimination of lubrication and friction dependent joints
inadequate force or torque margin of safety	accurate analysis methods; redundancy in actuation and motion possible
lack of accurate modeling and analysis methods for flexible and large-displacement segments	proven design and analysis methods
reduced reliability in off-nominal conditions	analysis methods provide increased predictability of behavior in off-nominal conditions; reduced susceptibility to foreign objects during testing and operation
thermal gradients cause joint binding or misalignment	mechanisms constructed of a single continuous material
backlash, hysteresis, and joint misalignment	monolithic (single piece) nature of compliant joints eliminates backlash, makes hysteresis predictable, and reduces the need for assembly, thus reducing the possibility of joint misalignment

These advantages eliminate or reduce many of the disadvantages inherent in rigid-link space mechanisms. CMs also offer an increased number of mechanism designs, joints, and configurations. This provides more options in finding an optimized, low-cost mechanism design. The distributed compliance of some CMs could be particularly useful in robotic grasping, sample collection, landing platforms, and rover suspensions. Overall, the advantages of compliant space mechanisms provide the opportunity to design simpler, more reliable, better performing, and more cost-effective solutions for many space applications [4].

This numerous advantages also come with some challenges. Two distinct challenges are that the coupling of motion and forces in CMs creates a more complex design situation, and the fact that off-axis stiffness and motion are possible [4].

Typically, a mechanism is designed so it can achieve a certain motion. Then, the forces in the joints and links are determined. However in CMs, the kinematics and dynamics are coupled. Moreover, in current space mechanisms, off-axis stiffness are significantly larger than the stiffness in the desired direction/axis, and hence they are often neglected. In CMs, off-axis stiffness can be lower and could create undesirable parasitic motion [4]. Another significant challenge is the design of thin flexible segments to withstand the vacuum and thermal extremes of space [7].

Fortunately, these challenges are surmountable if proper attention is given to already established compliant mechanism design and analysis guidelines. Some aspects, such as manufacturing and testing, will involve a certain level of difficulty due to the stringent requirements for space applications [4].

2.3   Space mechanisms

Many earth-sensing satellites, planetary rovers and orbiters, and manned spacecraft have been developed that require mechanisms to perform specific tasks, such as deployments, instrument pointing, stage separations, dockings, sample return, landings, retention and release, attitude stability, etc [4].

Since the general paradigm for designing space mechanisms has remained fairly consistent over the years, design rules exist for space mechanisms and have been generally well established by industry. The NASA Space Mechanisms Handbook is the space industry's authoritative document on space mechanism design and contains guidelines and details for space mechanisms of all types [8]. The AIAA has a similar document that standardizes how to, for example, calculate margins of safety for a space mechanism and is commonly used in the space industry [9]. Research needs to be performed in collaboration with these knowledge standards [4]. Table 2.2 lists different types of mechanisms needed in space, most of which are identified in the NASA Space Mechanisms Handbook.

Table 2.2: Space Mechanism Types. Extracted from [4].

Space Mechanism Types		
Deployable	Rotating	Suspension
Restraint and Release	Latches and Stops	Drive
Vibration Isolation	Separation	Landing
Sample Return	Docking	Shape Control
Pointing/Oscillating		

Besides, the NASA Technology Roadmaps provide specific areas where CMs may make an immediate impact and help to show how research in this field contributes to technological goals on a national level [4, 10]. Technology Roadmaps 12 and 9 are most applicable to compliant space mechanisms. Technology Roadmap 12, "Materials, Structures, Mechanical Systems, and Manufacturing" [10] provides detailed technologies that are priority for research and development in the areas most related to compliant mechanisms. Several of the identified technologies are listed in Table 2.3 [4].

Table 2.3: Technologies Identified for Future Development by NASA Technology Roadmap 12. Extracted from [10].

Roadmap Section	Subsection	Specific Technologies Identified
12.1 Materials	Flexible Material Systems	Expandable Habitat; Flexible EDL Materials; Solar Sail; Shape Morphing Materials; Advanced Expandable Materials
12.2 Structures	Lightweight Concepts	Composite/Inflatable Habitats; Expandable Structures (Precision Mirrors and Solar/Antenna Arrays); Landers
12.2 Structures	Innovative, Multifunctional Concepts	Reusable Modular Components
12.3 Mechanical Systems	Deployables, Docking and Interfaces	Common Universal Interchangeable Interfaces; Restraint/Release Devices; Deployment of Flex Materials; Large Lightweight Stiff Deployable; Precision Structure Deploy Mechanism
12.3 Mechanical Systems	Electro-mechanical, Mechanical and Micromechanisms	Active Landing Attenuation System; New Concepts
12.3 Mechanical Systems	Design and Analysis Tools and Methods	Kinematics and Rotor Dynamics Analysis

Lately, Technology Roadmap 9 "Entry, Descent, and Landing" [11] also provides areas for application of compliant space mechanisms, such as: flexible thermal protection systems for entry; mechanical deployments for attached deployable decelerators for descent; and anchoring, touchdown, and extreme terrain suspension systems for landing [4].

2.3.1 Compliant space mechanisms

Although not yet widespread, flexible links have been successfully used on space mechanisms and the field is just beginning to be explored [12, 13]. Compliant vibration isolation systems such as SoftRide are produced by CSA Engineering (a division of Moog), and these have been used on numerous satellite missions [14] .
Figure 2.1 show these compliant mechanisms being effectively used to isolate a satellite from launch vehicle vibrations. Similar mechanisms have been used on the Hubble Space Telescope for on-orbit jitter reduction and solar array vibration damping. Propellant tank tab flexures and compliant universal joints are other common examples [4].
The mechanism in Figure 2.1 was designed and tested successfully for damping the vibration generated in the process. The design parameters are considered to replace the existing mechanism with a new compliant one; the joints can withstand high-temperature gradients, statically balance joints, high tolerance of deflection of joints (+90 to -90 degrees) [15].
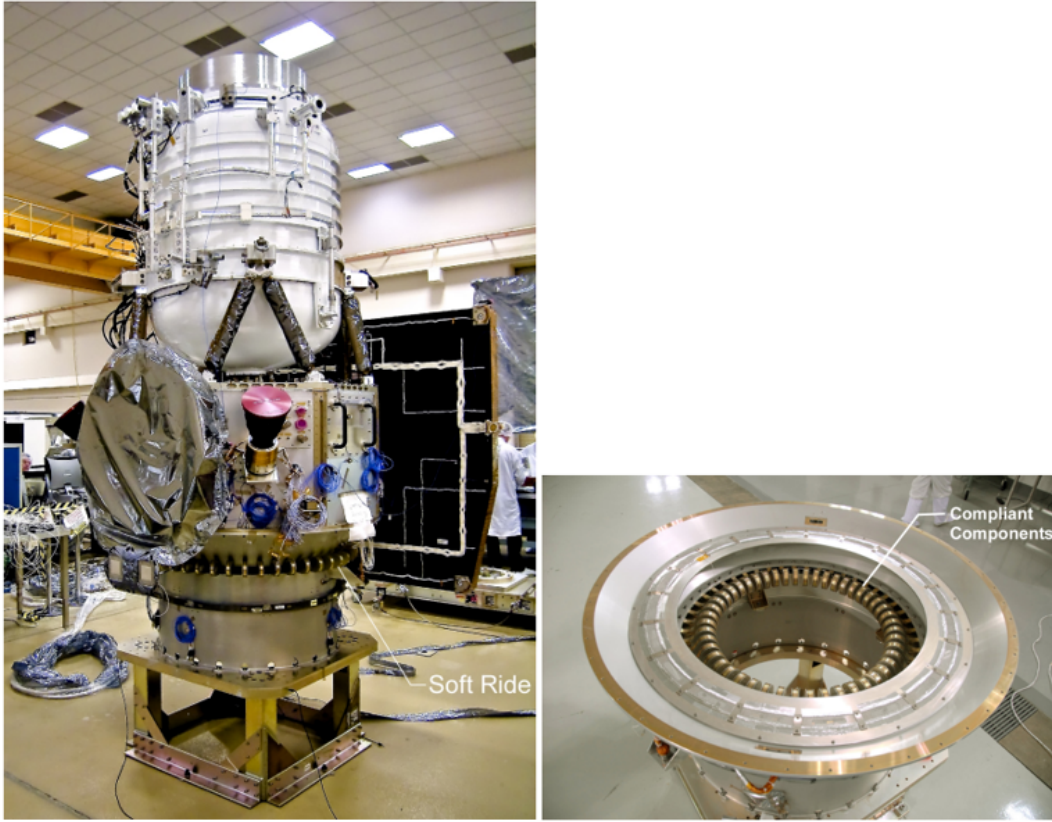
Figure 2.1: On the left, example of a compliant space mechanism. SoftRide vibration isolation mechanism. The compliant segments separate the launch vehicle adapter and the satellite WISE that was launched on a Delta II in December 2009. On the right, another example of a compliant space mechanism. SoftRide vibration isolation mechanism. Extracted from [4].

Moog CSA's SoftRide vibration isolation systems protect whole satellites from the rough ride into orbit. SoftRide also provides some shock isolation and reduces transmission of energy that drives acoustic loading [14].

Figure 2.2: SoftRide vibration isolation mechanism. Extracted from [14].

The problems of outgassing, cold welding, and limited means of heat transfer created by the vacuum of space can be mitigated by using full CMs to eliminate, for instance, joint clearance or lubrication, as commented in previous sections [16]. Furthermore, CMs have been used for efficient energy harvesting, vibration isolation, or suppressing resonant vibrations (as seen in Figure 2.1) by using their nonlinear load-displacement characteristics such as negative stiffness and load-stiffening [16].

2.4 Applications of Compliant Mechanisms

Compliant mechanisms can be used in a variety of promising applications in both micro and macro scales, especially where high-precision motions are required. These emerging applications can fall into six fields, which are detailed in Figure 2.3.
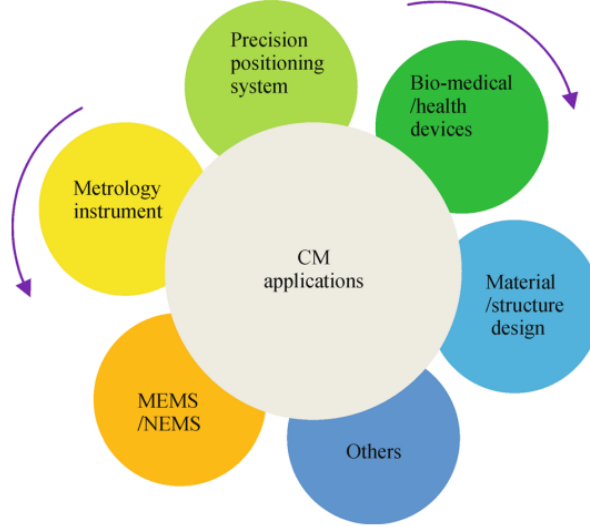
Figure 2.3: Applications of Compliant Mechanisms. Extracted from [16].

As previously mentioned, the NASA Space Mechanisms Handbook provides comprehensive identification of various mechanisms required in space applications [8]. This section will now showcase specific instances of CMs employed within such mechanisms, as outlined in the aforementioned Table 2.2.

Deployable space structures

Deployable space structure technology is the optimal solution for addressing engineering problems in the field of aerospace, which is the frontier field of engineering research. What is more, it is a potential approach to solve the contradiction between the requirements of large-scale spacecraft structures and the envelope limitation of a rocket launch [17]. Deployable structures can be comprised of bistable mechanisms or tape springs to effectively fulfill their primary function.

On one hand, a compliant bistable mechanism has two stable equilibrium positions. The bistable mechanisms will tend to one of two positions if no external forces are acting on it. Each stable position represents the local potential energy minimum, called the potential energy wells. A specific amount of external energy is required if the compliant bistable mechanism jumps from one stable position to another. This energy is called an energy barrier between two potential wells. Additionally, there is a certain distance between two equilibrium positions. This distance can change the overall dimensions of the structure, accordingly making the structure deployable. In addition, this distance determines the deformation ability of the deployable structure [18]. Figure 2.4 shows an example of a deployable structure designed with a compliant bistable mechanism.

Figure 2.4: Cylindrical deployable structure. Extracted from [18].

On the other hand, tape springs are mainly used in space deployable structures for satellites. Indeed, they represent simple, autonomous, robust and easy-to-integrate components compared to common mechanisms usually composed of several kinematic joints set into motion by the means of motors [19]. Figure 2.5 and Figure 2.6 show examples of deployable structures based on tape springs.

Successful uses of tape springs can be found in several space missions such as the six MYRIADE micro-satellites for the deployment of solar arrays, antennas and masts [20, 21]. Also, the MARS EXPRESS spacecraft used tape springs for the deployment of a long wavelength antenna [22, 23]. Lastly, tape springs will be found in future missions such as SOLAR ORBITER for the deployment of a radio and plasma wave antenna or NORSAT-1 for the deployment of an AIS (Automatic Identification System) receiver [19].

They are also considered as support structures for the deployment of Cassegrain telescopes, inflatable structures and solar sails [24, 25, 26, 27].
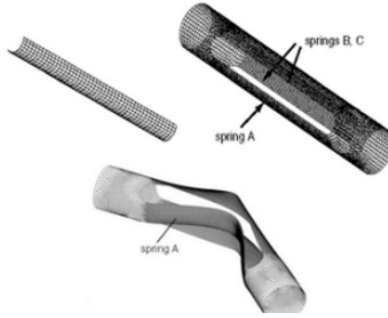
Figure 2.5: Tube hinge with three cutting slots. Extracted from [28].
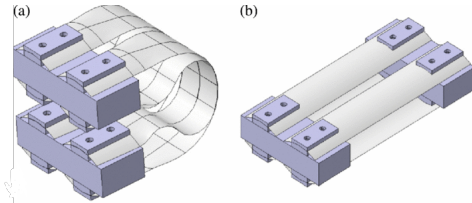
Figure 2.6: Tape springs folded (a) and extended (b) position. Extracted from [29].

As an example, the mechanism shown in Figure 2.6 is studied in the context of solar panel deployment applications [30]. Furthermore, it is worth noting that further investigations can be undertaken concerning CMs to uncover additional applications, including those pertaining to space orbit missions or the provision of support for space inflatable structures (refer to the references cited in article [19]).

Restraint and release space structures

The Apollo missions, the only crewed lunar missions performed so far, provided an enormous amount of data about the Moon. One of the aspects which had a substantial impact on hardware operations was lunar dust. During the Apollo operations, particles smaller than 2 μm proved to be the most problematic. The fragments of this size are able to enter hardware gaps, clearances and backlashes between hardware elements, causing the increase of friction and decrease of performance. Furthermore, the minerals present in the dust, such as anorthite, bytownite, labradorite, fayalite or forsterite, score 6 and above on the Mohs scale of minerals hardness. As for comparison, most steel alloys score 4–4.5 on the same scale. This means that the engineering materials of the hardware are exposed to sharp particles consisting of harder materials, leading to the risk of abrasive wear. Some examples of dust-related damage of mechanisms mentioned in the Apollo de-briefing reports and discussed in the literature are presented in Table 2.4 [31].

Table 2.4: Apollo mechanisms dust-related problems based on the astronaut de-briefings. Extracted from [32].

Mission	Problem
Apollo 12	Lock buttons of the equipment conveyor very hard to manipulate because of the dust accumulation in the moving parts
Apollo 15	Camera drive mechanisms got jammed with dust and prevented it from working
Apollo 16	Battery cover of radiator jammed because of dust accumulation in the mechanism
Apollo 17	Some of the moving components of the geopallet got stuck after the second EVA; the angle adjustment of some geological tools (scoop and rake) got fixed in one position which could not be changed anymore; multiple components attached to the rover jammed because of the dust exposure (e.g. bag holders, pallet locks)

An example of conventional rigid body hinge compared to compliant hinge designs is presented in Figure 2.7. The input work supplied to a CMs is partially stored as elastic energy in the material, and once the input is removed the mechanism can spring back to its original shape. This makes CMs particularly well suited to replace traditional spring loaded mechanisms [31].
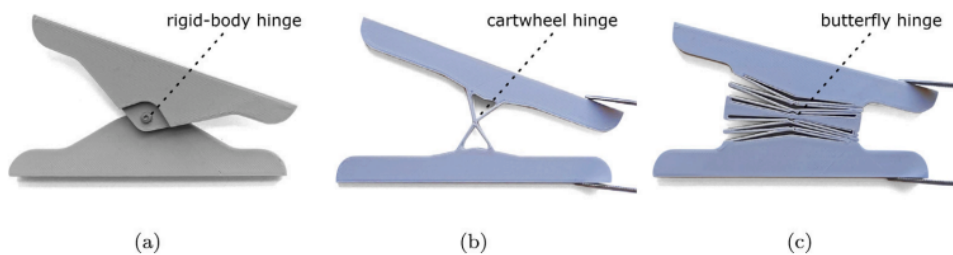
Figure 2.7: Rigid body hinge (a), and various designs of compliant hinges (b) and (c). Extracted from [31].

One of the geological tools from the Apollo program, namely the Tongs, is reproduced using CMs in literature [31]. This has been a critical tool for the Apollo missions since the astronauts' spacesuits did not provide enough dexterity to allow them to pick up rock samples from the ground without any tools. The Tongs (Figure 2.8) were used to collect rock samples with diameters smaller than 10 cm.

Figure 2.8: The training replica of Apollo Tongs, photographed in ESA's European Astronaut Centre Extracted from [31].

The proposed solution is to use an alternative design methodology where all the inter-element gaps are eliminated, and traditional mechanisms are replaced with CMs [31]. The Figure 2.9 shows a rigid body hinge and two possibles re-designs using CMs.

(a) Default position. (b) Open position. (c) Close position.

Figure 2.9: Various deflection stages of the TPC gripper with undeformed blue shape visible in the background. Extracted from [31].

On the other hand, CMs can achieve bistable motion without bearings or friction. They can be designed to provide precise state positions. Compliant bistable mechanisms, such as that shown in Figure 2.10, have potential application in space systems as switches, latches, or as an alternative to pyromechanical release devices [33].
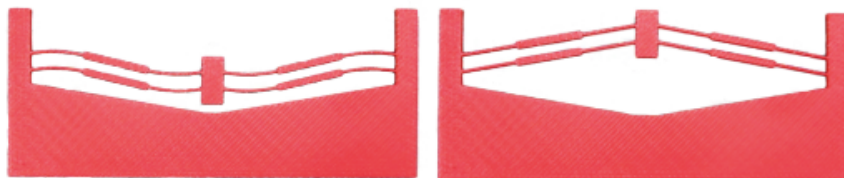
Figure 2.10: Bistable mechanism prototyped in ABS plastic, using a Dimension SST 1200ES 3D Printer. Extracted from [33].

Compliant bistable release mechanisms can be used as non-explosive release mechanisms at a fraction of the cost and weight of traditional release mechanisms.

Therefore, it would eliminate the challenges of having explosive charges on the spacecraft. They can be compact compared to other alternatives, thereby reducing weight. They will enable systems to be testable and resettable [33].

Compliant mechanisms for shape control

Starting in 1998, CM technology was first applied to the wing morphing problem. Working with funding from the AFRL Air Vehicle Directorate, a compliant variable camber wing leading edge (a 3-foot NACA63418 profile embedded with CM) was designed, fabricated, and tested. The leading edge CM is designed to withstand the external air-loads while producing a 0 to 6 degree change in camber. Wind tunnel test results showed a 51% increase in lift-to-drag ratio and a 25% increase in the lift coefficient for the 6-deg leading edge camber change, see Figure 2.11 [34].

Figure 2.11: Adaptive Compliant Wing with an embedded compliant mechanism provided 6-degree leading edge camber change on demand. Wind Tunnel test results showed a 51% increase in lift-to-drag ratio and a 25% increase in the lift coefficient for a 6-deg. LE camber. Extracted from [34].

Nowadays, extensive investigations have been conducted within this domain, leading to the discovery of novel technologies.

Lockable devices are a kind of key components in robotic systems and adaptive structures, which can be utilized to achieve energy management and/or structure reconfiguration. For a geometry variable truss system, lockable devices can be used to achieve its reconfiguration between a truss and a mechanism [35]. A new modular lockable prismatic (P) joint based on a CM is shown in Figure 2.12.
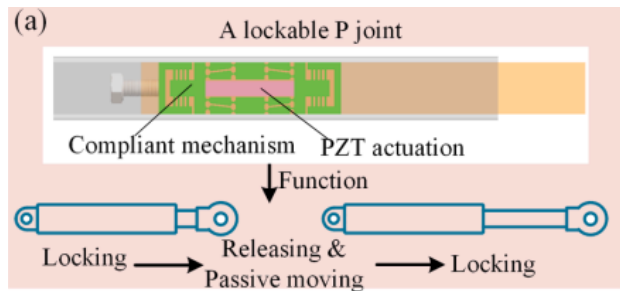
Figure 2.12: Compliant mechanism design for shape control. Extracted from [35].

One of the immediate applications of the design is the reconfigurable variable geometry truss (VGT) systems. In this application, many compact and lightweight lockable P joints are needed to construct a passive lockable load-bearing structure for an adaptive trailing edge. Different kinds of motion modes can be obtained by releasing specific joints to make the trailing edge reach desired shapes through active skins actuation [35].
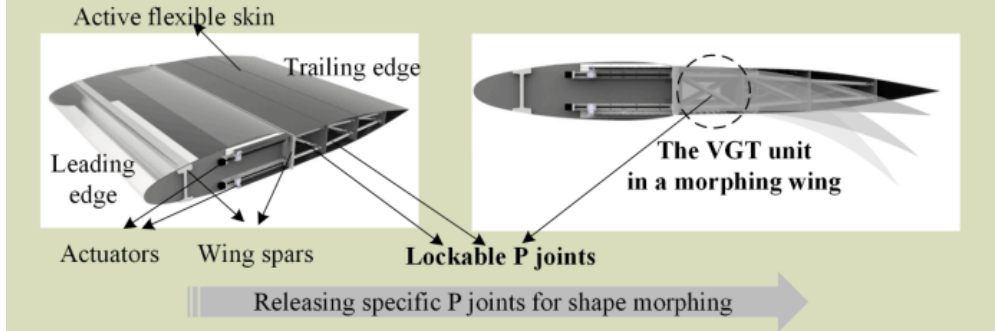
Figure 2.13: Application of CMs on shape control. Extracted from [35].

In Figure 2.13 a design prototype of this application is exposed, which is actuated by two linear motion modules in which the sliding platforms are connected with flexible limbs [36].

In this context, the term adaptive compliant wing is to be understood as an aircraft wing morphing its geometry in flight without losing the surface integrity and without the elements of the "gapped" flap system. Some designs proposed for the adaptive compliant wing frame are based on the use of the reconfigurable honeycomb core combined with actuators intended to ensure the elements of the wing structure will be reciprocally and concordantly repositioned at a given angle, as shown in Figure 2.14 [37]. The reconfigurable honeycomb core of an adaptive compliant wing is a controllable dynamic spatial structure with flexible cell jointing in the form of joints with the hidden topological surfaces.
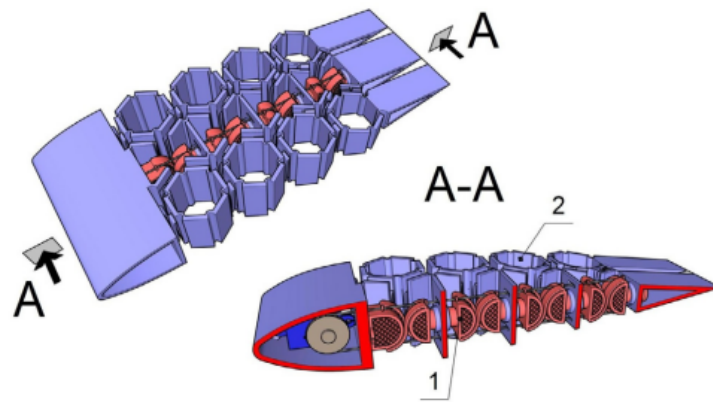
Figure 2.14: Reconfigurable honeycomb core fragment diagram of the adaptive compliant wing with the integrated mechatronic node. Extracted from [37].

An adaptive compliant wing can considerably increase the aircraft aerodynamic quality and enhance its maneuverability, fuel efficiency, engineering-and-economic performance as well as improve the aircraft functionality as compared with the conventional wing system [37].

In addition, adaptive compliant wings can be most relevantly applied in supersonic aircraft, short takeoff and landing (STOL) aircraft, and aircraft with optimal aerodynamics in various flight modes [37].

Pointing / oscillating space structures

Another design for space applications accomplished using CMs is a monolithic 2-DOF fully compliant space pointing mechanism. A pointer is a mechanism that has the capability to orient an output stage along one or more axes. Pointing mechanisms have wide applications in spacecraft design. In space, the capability of pointing a thruster could eliminate the need for multiple thruster arrays, reducing part count and potential failure points. The ability to accurately point a communications antenna could decrease the power required to send data. Similarly, pointing a solar array would give the ability to orient it for optimal capturing of solar radiation, increasing efficiency of energy capture [38].

Figure 2.15 shows the pointer mechanism developed in an effort to incorporate compliant mechanism design in a space-centered application [38].
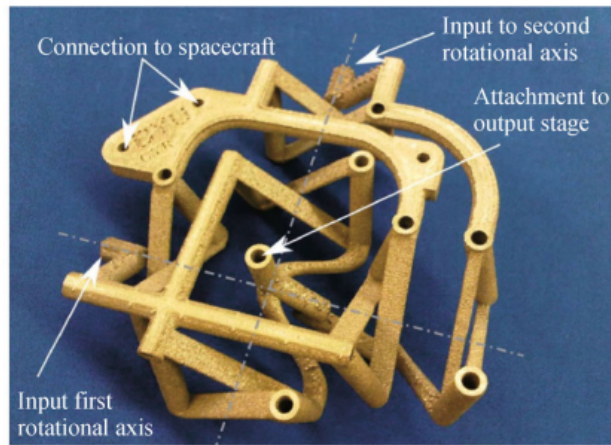
Figure 2.15: Monolithic 2-DOF fully compliant space pointing mechanism. Extracted from [38].

Numerous mechanism topologies were evaluated and a five-bar spherical mechanism was selected for the pointer mechanism. It requires only two actuators and can passively support the applied thruster load as seen in Figure 2.16.

Figure 2.16: The pointer mechanism integrated with a small attitude control thruster demonstrating compliant mechanism design in a space-centered application. Extracted from [38].

The performance of the pointer mechanism shows that combining compliant mechanisms with the manufacturing capabilities of 3-D printing has the potential to influence the way space mechanisms are designed [38].

Compliant mechanisms for separation

The Monolithic tools and devices with bi-stable mechanisms are very useful in space applications with stable and consistent deflection, as mentioned before. Rapid motion is achieved when actuated as the energy release is constant and significant. The permissible stress had a high range that can withstand a million repetitions that would be promising in the further development of aerospace application in monolithic devices [15]. This tools can be applied in satellites, for instance as shown in Figure 2.17.
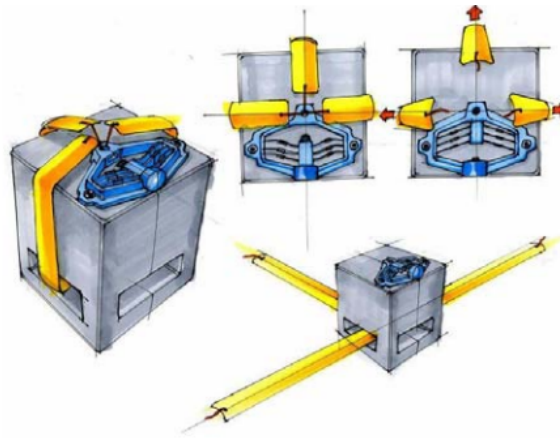
Figure 2.17: The application of a Bi-stable wire cutter device applied to a satellite for the deployment of segments. Extracted from [15].

The Cubesat satellites (ESA) used very complex mechanisms for the deployment of solar panels arrays. Contrarily, Figure 2.17 shows the release of flexural material with internally stored energy, which is released when the bistable Mechanism's blade moves it to its second stable position by cutting the string, resulting in the deployment.

Compliant mechanisms for vibration isolation

Vibrations are produced in machines that have unbalanced masses. These vibrations will be transmitted to the foundation upon which the machines are installed and are usually undesirable because it can affect the functioning of the machine. Vibration isolation reduces the level of vibration transmitted to or from a machine, mechanism, or structure from another source [39].
CMs is the focus of active research because of the stability, robustness, and ease of manufacturing endowed by their unitized construction. In Figure 2.18, an application of compliant mechanism for a vibration isolation system with a rigid foundation is explored. The structural optimization approach is focused on the determination of the topology, shape, and size of the mechanism. The building blocks are used to optimize a structure for force transmission [39].
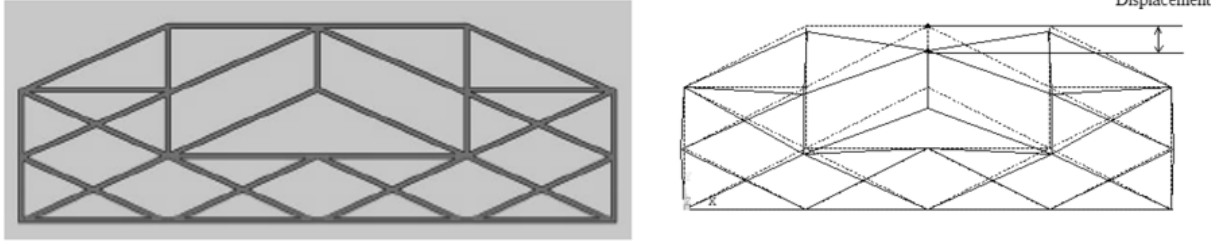
Figure 2.18: On the left, the compliant isolator design. On the right, the displacement transmissibility for various frequency ratios. Extracted from [39].

On the other hand, a novel compliant positioning stage with low-frequency vibration isolation capability is developed in literature [40]. It adopts a symmetry design, shown in Figure 2.19, which combines a stretching mechanism and four quarter bridge-principle amplifiers to realize the large amplification ratio, meanwhile utilizes a giant magnetostrictive actuator (GMA) to obtain the capabilities of ultra-precision positioning and vibration isolation in low frequency.
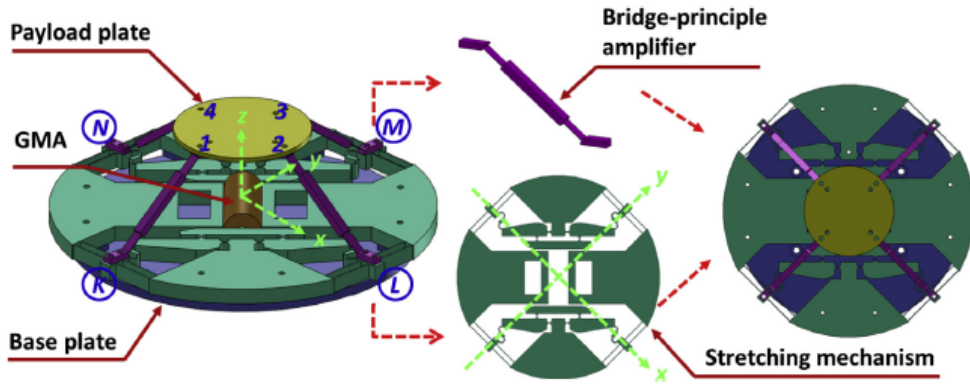
Figure 2.19: Conceptual scheme of the z-directional positioning stage. Extracted from [40].

The corresponding performance is validated by finite element analysis, the prototype is fabricated and experimental tests are conducted to investigate the factual performance [40]. The test results demonstrate that the amplification ratio could be up to 4.15 which matches well with the simulation value 4.18. The natural frequencies along the z-direction are tested to be 458 Hz, which is 3.4% higher than the simulation result. The positioning performance tests show that the actual positioning trajectories track well with the desired sinusoidal trajectories in different driving frequencies, which means a good positioning capability. In addition, the vibration isolation effect in low frequency is evaluated and the results confirm that nearly -15.8 dB vibration attenuation could be realized under the harmonic disturbance which shows a bright future in aerospace engineering. [40]

Drive space structures

A compliant variable diameter mechanism useful in variable diameter wheels is shown in Figure 2.20 [41]. The mechanism proposed allows the rover wheels to transform its structure using contraction expansion-retraction motion and gives excellent running performance to it. Compliant variable diameter mechanism prevents

backlash, wear, need of lubrication, simplifies assembly, makes mechanism more lightweight as well as compact compared to the conventional rigid body mechanism. Hence this compliant variable diameter mechanism is useful for creating variable diameter wheels for the application of lunar rover [42].
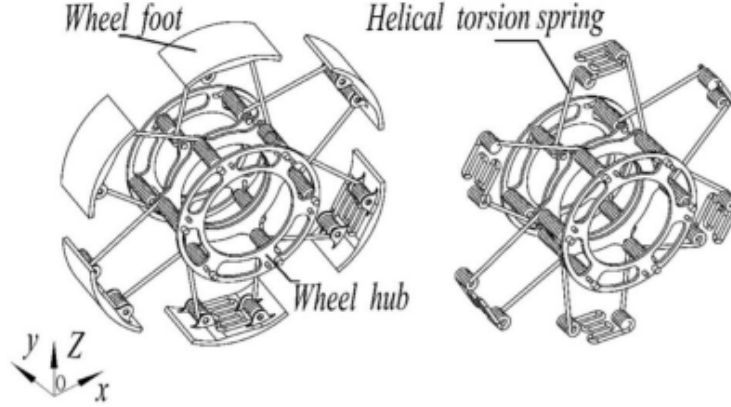
Figure 2.20: Compliant variable diameter mechanism Extracted from [41].

2.4.1 Compliant mechanisms in the biomedical field

Compliant mechanisms are well suited for application in biomedical applications because of their low wear, the ability to be fabricated of bio-compatible materials, and their compactness. There are many possible research areas and applications, and one implant is described in [3].

The design objective of the spinal implant is to restore healthy physiologic biomechanics to the degenerated spinal segment. A CM was designed as a spinal implant to share load with a damaged or diseased intervertebral spinal disc, as shown in Figure 2.21.
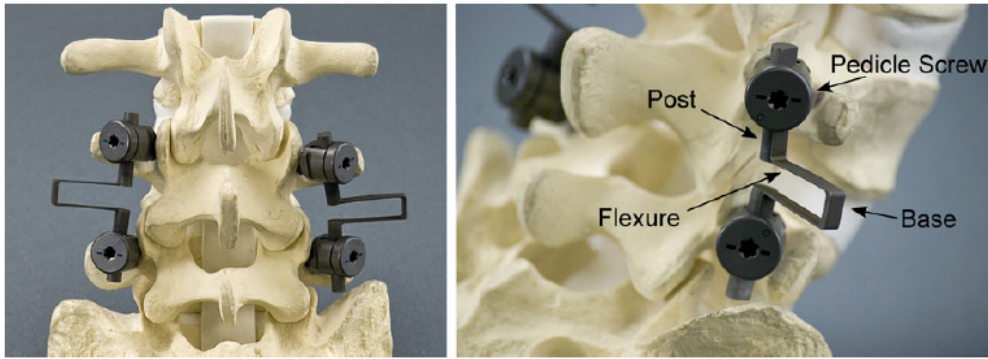
Figure 2.21: Prototype of the baseline configuration. Extracted from [3].

The baseline configuration of the spinal implant is based on the Lamina Emergent Torsional (LET) joint. The LET geometry offers advantages in terms of manufacturability and independently controlled flexibility in multiple directions. The device consists of a LET joint that has been split into two parts that are independently attached to the vertebral pedicles. The vertebra themselves act as semi-rigid connections between the two parts of the LET joint. Figure 2.22 shows the baseline configuration deflected in the two modes of loading for which it was designed [3].
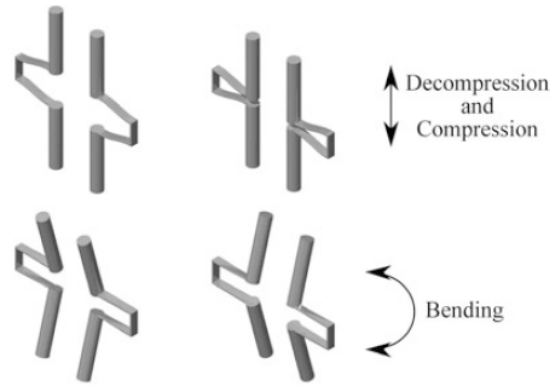
Figure 2.22: Deflected positions of the baseline configuration. Extracted from [3].

Lastly, another application of CM in the biomedical field consists in Minimally Invasive Surgery (MIS) which has revolutionized surgery by allowing operations to be conducted through incisions of a few millimeters utilizing thin, flexible instruments. Such operations lead to shorter hospital stays, less cost, and less scarring. Minimally invasive implies a set of surgical techniques in which special instrumentation allows surgeons to perform complicated operations via small incisions in a patient's side, rather than through large cavities, as in traditional open surgery. Surgical instruments based on CM offer a number of potential advantages over traditional MIS instruments and the current robotic systems [43].

The designs postulated for surgical compliant tools encompass a macroscopic-scale compliant gripper and a compliant kidney manipulator.

Chapter 3

Introduction to Topology Optimization

The primary focus of this study is CMs design in Topology Optimization (TO). While alternative methods have been used in the past, TO has become a cutting-edge technology in this field in recent years and it is being actively studied to find new innovations. For this reason, this study has focused on TO as a method of designing CMs and other methodologies are not considered. In this section, a comprehensive theoretical background on TO is presented and the design methodology of CMs is explained.

The majority of structures contain a significant amount of superfluous material that could be eliminated with a more optimal design. The goal of TO is to propose, design or improve structures by finding designs that can guarantee equal stress, strain, or any material physical property of a structure while using less material. Furthermore, because this technology involves the removal of material from structures, it is of particular interest to the aerospace industry, which faces a significant challenge in achieving lighter designs. Nowadays, TO is implemented in a variety of scientific fields as thermal process, fluid dynamics, physics or engineering, for instance [44].

3.1   The topology optimization problem

A topology optimization problem inherently encompasses a minimization problem in which a cost function, typically denoted as $J(x)$, and constraints (either equality, inequality or box constraints) need to be specified. For instance, we can postulate the minimization of the structural volume, $J(x)$, while simultaneously ensuring that the stress remains below the plastic stress. In certain problem domains, a discretized form of a Partial Differential Equation (PDE) constraint may arise, manifesting as the equilibrium equation for the structural system.

Example of a generic topology optimization problem:

$$
\begin{aligned}
\min_{x} \quad & J(u(x), x); && \text{cost,} \\
\text{s.t.} \quad & A(x)u = b(x); && \text{PDE constraint,} \\
& h_i(x) = 0; && \text{equality constraint,} \\
& g_j(x) \leq 0; && \text{inequality constraint,} \\
& 0 \leq x \leq 1; && \text{box constraint.}
\end{aligned}
\tag{3.1}
$$

For the sake of simplicity, the term $J(u(x), x)$ will be denoted as $J(x)$ henceforth. It is important to acknowledge that the cost $J(x)$ represents a shape functional, meaning an operation that accepts a function as input and yields a real number as output.

In topology optimization problems, a computational domain is usually defined in the following manner

$$
\Omega = \{x \in D \; ; \; x = 1\}
\tag{3.2}
$$

where D is the reference domain and Ω the material domain. The assignment of black color is conventionally associated with $x = 1$ values, while white color corresponds to $x = 0$ values. Herein, we introduce the designation of Ω as the ultimate design represented by black, x that denotes a spatial point, and D that represents the total bounding box. Consequently, Ω comprises the aggregate set of points within the domain that equate to 1. The design variable x is commonly referred to as the characteristic function χ in the context of structural problems.

3.2 Topology optimization limitations

The primary challenge in TO lies in the absence of pre-existing solutions, needing the incorporation of constraints. For instance, consider the establishment of a structure characterized by a pulling force exerted from both sides. The objective is to attain a volume equivalent to 50% of the entire domain D while maximizing its stiffness to the greatest extent possible.

Figure 3.1: Optimal solution to the problem.

The structure shown in Figure 3.1 represents an optimal solution; nevertheless, it is worth noting that an alternative solution also achieves optimality, as seen in Figure 3.2.
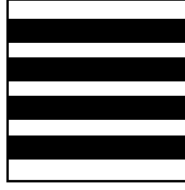
Figure 3.2: Alternative optimal solution to the problem.

It becomes evident that when the number of horizontal bars is doubled while simultaneously reducing the volume allocated to each bar by half, an infinite set of optimal solutions arises for this particular problem, with higher stiffness as the amount of bars increases. In order to address this and, thus, ensure the presence of feasible solutions, the introduction of a perimeter constraint can be considered to limit the solutions within a defined boundary.

Introduction of a perimeter constraint to a topology optimization problem example:

$$
\begin{aligned}
\min_{x} \quad & J(x) + \alpha Per(x) \ , \\
\text{s.t} \quad & h_i(x) = 0, \\
& g_j(x) \le 0,
\end{aligned}
\tag{3.3}
$$

where α represents a penalty coefficient for the perimeter constraint, which serves as a limiting factor to prevent the solutions from reaching excessively high values of perimeter and, consequently, the solutions are truncated at a specific point.

An alternative approach to address the issue of non-existent solutions is through the use of a technique known as Filtering. This process involves computing the average of the characteristic function values within the continuous range of 0 and 1, the extent of which relies on the size of the applied filter. By employing a filter, an intermediate zone (referred to as grey) is established between the black and white boundaries, transforming the domain from a state of discontinuity to continuity. These grey zones encompass values ranging between 0 and 1, facilitating the existence of solutions by effectively mitigating smaller scales. That is why the resulting field, which will serve as an additional tool to compute shape functionals (not a new design variable), will be referred as regularized density.

When implementing a filter with a specific size the resulting outcome manifests as shown in Figure 3.3.
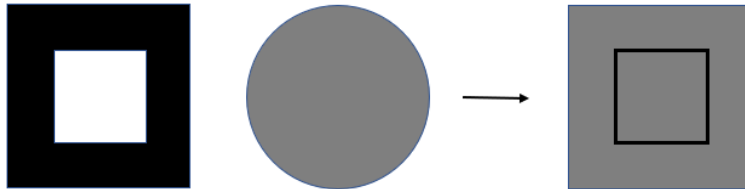
Figure 3.3: Result of the implementation of the Filtering approach.

However, when employing a smaller-sized filter the resultant outcome yields a distinct solution depicted in Figure 3.4.
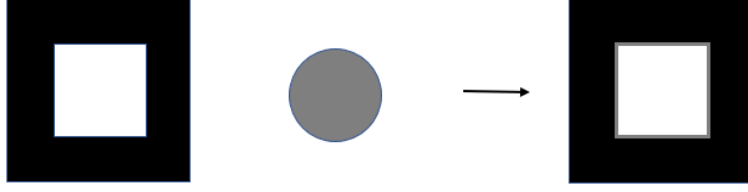
Figure 3.4: Alternative solution of the implementation of the Filtering approach employing a smaller-sized filter.

It is important to emphasize that the filter should be kept as limited as feasible to avoid the risk of information loss. Using excessively large filters may compromise the accuracy and fidelity of the results obtained.

3.3 Density and level set approach

The main limitation of the original problem lies in the discrete nature of the design variable χ. As a result, derivatives are non-existent at the boundaries between white and black values. To overcome this limitation, various methodologies have been proposed to substitute χ with an alternative design variable.

Among all the exiting methods developed for topology optimization, the two most prominent are the density-based SIMP method and the Level Set method.
To achieve a comprehensive understanding of both methods, it is essential to revisit the definition of χ, shown bellow

$$\chi\left(x_i\right) = \begin{cases} 1 & \text{if } x_i \in \Omega \\ 0 & \text{if } x_i \notin \Omega \end{cases}, \tag{3.4}$$

where x_i denotes a position within the reference domain D. Due to χ is constrained to assume only values of 0 or 1 a more flexible formulation is introduced for the problem: the density approach.

3.3.1 Density approach

In this context, the variable x from the original problem, representing the quantity we aim to minimize, is designated as the density ρ. Therefore, the problem can be defined as follows.

Example of a structural topology optimization problem implementing a density approach:

$$
\begin{aligned}
& \min_{\rho,\, u} && J(\rho) = f \cdot u(\rho) \\
& \text{s.t} && K(\rho) \cdot u = f \\
& && V(\rho) \leq V^* \\
& && 0 \leq \rho \leq 1
\end{aligned}
\tag{3.5}
$$

where the PDE constraint $K(\rho) \cdot u = f$ refers to the structural equilibrium equation discretized with finite

elements, K is the stiffness matrix, f the external forces vector, u the displacement vector and V the volume. Here, the cost used is known as the compliance $c = f \cdot u$, a measure for the structural flexibility.

The density variable now spans a range between 0 and 1, expanding beyond the restriction of exclusively assuming one of these two values. Hence, it can be asserted that a relaxation of the problem has been accomplished with the introduction of grey values. The primary objective of this problem is to determine the optimal values for both density and displacements, such that the resulting displacements are minimized when subjected to an applied force.

It is noteworthy to mention that in this specific problem, if the value of ρ is known, the corresponding value of u can be obtained by solving the system of equations. Is in such cases where the problem is categorized as a PDE-constrained optimization problem, as the constraint is represented by a partial differential equation.

Revisiting the aforementioned problem, it is compelling to expound upon the role played by ρ in the stiffness matrix. The partial differential equation represents the strong form of the problem. To facilitate the discretization of the problem and acquire a solution, it is advantageous to transform the problem from the strong form to the weak form or variational problem. This transition allows for the formulation of a system of equations (typically algebraic in the form of $A \cdot u = b$) through discretization, enabling the attainment of a solution for the problem.

In the context of the elasticity problem, the strong form can be represented as follows

$$\nabla(\overline{\overline{C}} : \nabla^s u) = f, \tag{3.6}$$

wherein the constitutive tensor is denoted by $\overline{\overline{C}}$, the symmetric gradient of displacements is represented as $\nabla^s u$, and f stands for the applied force.

It is well-established that an alternative representation of the elasticity problem can be attained through the utilization of the following equivalent equation to define the stress tensor

$$\sigma = (\overline{\overline{C}} : \nabla^s u), \tag{3.7}$$

where $\nabla^s u$ is in fact the strain tensor ϵ. The elasticity problem has been formulated in its strong form; nevertheless, in the context of TO, it proves advantageous to transform it into the weak form, typically achieved by multiplying the strong form by a test function and integrating over the domain as

$$\int \nabla^s v : \overline{\overline{C}} : \nabla^s u = \int f v, \tag{3.8}$$

where v is defined as the test function. It will be now interesting to comment the significance of the weak form. To expound upon this matter, the following domain is proposed in Figure 3.5, wherein the unknown variables correspond to the displacements.
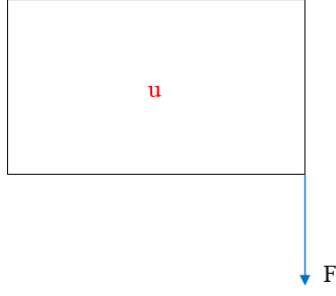
Figure 3.5: Proposed domain.

The displacements fields u is a function of spatial coordinate x, denoted as $u(x)$. It is crucial to acknowledge that obtaining the solution for every point of x_i through analytical means is unfeasible. Hence, the approach is to introduce a discretization in infinite elements that employs a combination of proposed functions to approximate the solution, with convergence being achieved as the number of shape functions increases. Therefore, the objective is to compute the value at a particular domain point and interpolate the remaining ones. This forenamed functions are represented as follows

$$u(x_i) = N_j(x_i)u_j, \quad \nabla u(x_i) = B_{Kj}(x_i)u_j, \tag{3.9}$$

$$v(x_i) = N_j(x_i)v_j, \quad \nabla v(x_i) = B_{Kj}(x_i)v_j, \tag{3.10}$$

where N_j can represent various types of functions, such as shape functions, exponential functions, or Fourier functions, among others; and B_{Kj} stands for the gradient of N_j. Consequently, if the evaluation of the solution is required at 10 distinct points, it necessitates the formulation of 10 equations to accommodate the 10 unknowns. The objective is to satisfy the strong form equation specifically for these 10 points in order to establish the weak form. This approach facilitates the integration of the individual equations for the unknowns, resulting in an averaging effect across the relevant regions. In this case proposed, the integration would encompass the fulfillment of 10 equations.

It is worth mentioning that the test function is usually represented with the same basis as the displacements, following the Galerkin method for finite elements.

The problem can now be reformulated employing the following terminology

$$\nabla^s v : \overline{\overline{C}} : \nabla^s u \rightarrow a(\rho, u, v), \tag{3.11}$$

$$fv \rightarrow l(v). \tag{3.12}$$

Here, the constitutive tensor $\overline{\overline{C}}$ is dependent on ρ through the Young modulus and the Poisson ratio. Thus, the problem can be reformulated according to the aforementioned nomenclature as follows

$$\min_{\rho, u} \quad l(u)$$

$$\text{s.t} \quad a(\rho, u, v) = l(v) \quad , \tag{3.13}$$
$$V(\rho) \leq V^*$$
$$0 \leq \rho \leq 1$$

which represents the problem to be addressed. It is worth noting that upon discretizing the problem, the connection between the constitutive tensor $\overline{\overline{C}}(\rho)$ and the variables u and F can be formulated as the equation $K(\rho)u = F$, since K integrates the constitutive tensor of each element assembled.

In contrast, the resolution of such problems can be accomplished through the use of the isotropic material with penalization approach or the SIMP method. The concept of problem relaxation is represented by the acceptance of intermediate gray values during the optimization process, with the ultimate requirement being the attainment of a final solution consisting solely of black and white values. To elaborate further on this notion, consider Figure 3.6.
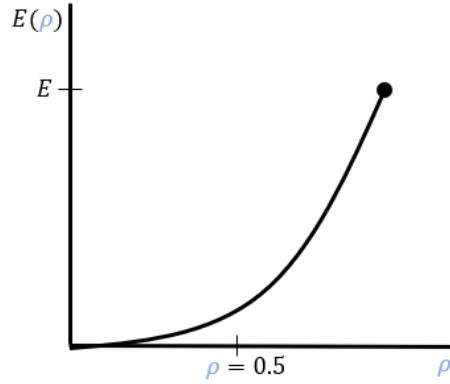
Figure 3.6: Representation of the density values regarding the Young modulus for a optimized structure.

The graph portrays the density values, denoted as ρ, in relation to the Young modulus, E, across various regions within the domain, Ω.

At the beginning of the graphic, white values are depicted, representing regions where the Young modulus is zero or extremely small. Conversely, at the opposite end, the point signifies the Young modulus value associated with the attainment of black values ($\chi = 1$). Note that it is required to define the Young modulus values for the intermediate range between 0 and 1. This is the aim of the SIMP method.

To ensure the ultimate achievement of solutions characterized by black and white values, meaning 0 or 1 values of ρ, it is necessary to propose competitive microstructures.

Definition of microstructure

As previously defined, an intermediate value of, for instance, $\rho = 0.5$ will be depicted as a gray region in the code; nevertheless, this value can also be represented through black and white solutions, which are referred to as microstructures, see Figure 3.7.

$\rho = 0.5$

$\rho = 0.5$
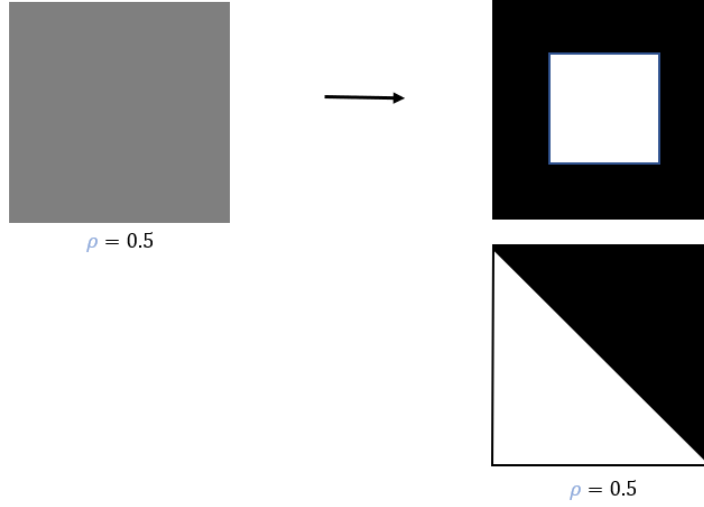
Figure 3.7: Representation of microstructures.

The homogenization of the two microstructures with $\rho = 0.5$ results in an identical solution (the left square). Conversely, when the process is reversed, an infinite number of microstructures can be generated. Considering this, the gray zones can be interpreted as the homogenization of a microstructure. It is worth noting that the distinguishing factor among these microstructures lies in the different value of their average Young modulus $\overline{E}$ or, in general, their constitutive tensor $\overline{\overline{C}}$.

Upon examining the graphic in Figure 3.6, it becomes apparent that the connection between the white and black values is not constrained and can assume infinite forms. Nevertheless, the SIMP method introduces a prescribed functional relationship for this connection, characterized by the following expression

$$\overline{\overline{C}}(\rho) = \rho^P \cdot \overline{\overline{C}}_0 \; ; \; P = 3, \tag{3.14}$$

where $\overline{\overline{C}}_0$ is the constitutive tensor of the black material ($\chi = 1$).

The proposed solution takes into consideration the relaxation of the problem, allowing for values between 0 and 1 while ultimately aiming for a final result composed solely of white or black zones. The function proposed exhibits a slight gradual increase in the elastic properties for density values ranging from 0 to 0.5, making these values highly noncompetitive for structural applications. Consequently, the emphasis is placed on values 0 or 1, which are considered the most competitive. By employing this function, it is ensured that the final result exclusively consists of white or black values, as intermediate values are penalized. This approach enables the relaxation of the problem during the intermediate stages, allowing for the inclusion of values between 0 and 1, thus defining a differentiable design variable.

This concept, wherein the code itself replaces the intermediate values with either white or black to obtain competitive solutions, is referred to as interpolation.

3.3.2 Level Set approach

To avoid the treatment of grey values of density, another alternative for the design variable is found. The concept revolves around parameterizing the problem using a level set Ψ function, to replace the original χ. Mathematically, it is expressed as follows.

$$\chi\left(\Psi\right) = \begin{cases} 1 \text{ if } \Psi(x_i) \leq 0 \\ 0 \text{ if } \Psi(x_i) > 0 \end{cases}. \tag{3.15}$$

It can be elucidated as a continuous and differentiable function whereby positive values within the domain correspond to white, while negative values or zero coincide with black values of the final result. As it can be observed at in Figure 3.8 this function can be also expressed in equivalent way with the Heaviside step function, as shown bellow

$$\chi(\Psi) = 1 - H_{\Psi>0}. \tag{3.16}$$
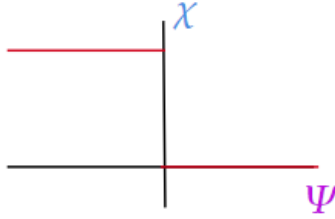
Figure 3.8: Graphic representation of χ when the characteristic function is replaced by the level set function.

The previously proposed problem with density was referred to as the extended, full, or monolithic problem, formulated in Equation 3.13.

Now, in the context of this problem, the variable u is dependent on χ, resulting in a single variable formulation. This gives rise to the reduced form of the problem, which can be expressed as follows:

$$\begin{aligned} \min_{\Psi, u} \quad & l(u(\Psi) \\ \text{s.t} \quad & V(\Psi) \leq V^* \end{aligned}. \tag{3.17}$$

Considering $u(\chi(\Psi)) \equiv u(\Psi)$ as a solution to the equation $a(\rho, u, v) = l(v)$, it becomes apparent that in this problem u is no longer regarded as a design variable by the optimizer. Instead, the focus is solely on χ as the variable of interest, which is defined with the new design variable Ψ. This approach is specifically applicable to problems with PDE constraints. It is worth emphasizing that the information regarding $u(\Psi)$ must be provided for this procedure. The Level Set method can be implemented using two distinct approaches, as seen in following sections.

Shape derivative

The concept aims to displace the boundary defining two states of the structure, see Figure 3.9. The shape derivative is precisely determined as the disparity between the two states, which can be interpreted as the linear variation or, the linear approximation of the cost when the boundaries of holes are moved a certain quality $\delta\chi$. Mathematically, this concept is expressed as follows

$$J_1(\chi) = J_0(\chi) + D_S J(\chi)\Delta\chi. \tag{3.18}$$
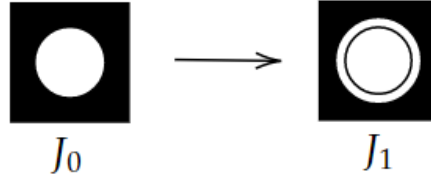
Figure 3.9: Graphic representation of the to states of the structure when implementing shape derivative.

Topological derivative

In an alternative implementation, the boundaries remain unchanged, and instead, the topology is modified by introducing an infinitesimal hole quantified by $\Delta\chi$, see in Figure 3.10. The topological derivative quantifies the variation in the cost resulting from the introduction of, for instance, a hole, providing insight into the sensitivity of the cost with respect to infinitesimal changes in the topology as

$$J_1(\chi) = J_0(\chi) + D_T J(\chi)\Delta\chi \tag{3.19}$$
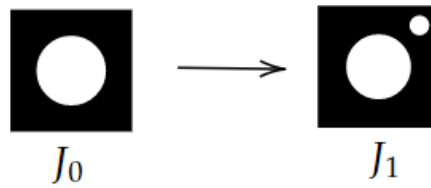
Figure 3.10: Graphic representation of the to states of the structure when implementing topological derivative.

The topological derivative possesses certain properties, which indicate that the following condition will be satisfied at the optimal point

$$\left.\begin{array}{l} D_T J(\chi) < 0 \rightarrow \chi = 1 \\ D_T J(\chi) > 0 \rightarrow \chi = 0 \end{array}\right\}. \tag{3.20}$$

This constraint is imposed to attain the optimal point. Consequently, it can be inferred that at the optimal point, $D_T J(\chi)$ is equivalent to Ψ. However, this process is highly rigorous, necessitating the proposal of certain procedures to relax the problem.

3.4 Reduced formulation and adjoint problem

As previously mentioned, when considering a topology optimization problem in the monolithic problem form, it involves two design variables. In this formulation, when using an optimizer, the resulting vector can become excessively large due to the requirement of gradients for each component. However, in the specific case of PDE-constrained optimization problems, it is possible to formulate a reduced problem that leads to a single variable formulation, as explained earlier. In this context, it becomes necessary to explore approaches for optimizing the variable χ, while solving for u as a linear system of equations. The only outcome of the PDE constrain is the redefinition of a new gradient for $J(\chi)$, concurrently diminishing the number of design variables exclusively to χ.

Thus, to address this problem, it is crucial to compute the total gradient, depending initially on χ and u. First, the previously established reduced problem will be reformulated into the canonical formulation. Mathematically and in the most general way, it is expressed as follows

$$
\begin{aligned}
&\min && j(x) = J(u(x), x) \\
&x && A(x) \cdot u = b(x) \\
&\text{s.t} && h(x) = 0 \\
& && x_{lb} \leq x \leq x_{ub}
\end{aligned}
\quad . \tag{3.21}
$$

The objective is to compute the gradient, $\nabla_x J$, when the cost function j depends on the variable x according to the expression shown above for the cost. This procedure is carried out by means of the adjoint problem, which can be formulated as the following sub-problem

$$
\begin{aligned}
&\min && J(u, x) \\
&x, u && \\
&\text{s.t} && A(x)u = b(x)
\end{aligned}
\quad . \tag{3.22}
$$

Given the invertibility of matrix A, the problem can be reformulated by replacing the cost function with a reduced cost function, resulting in a formulation with a single variable as shown bellow

$$
\min_x \ J(A(x)^{-1}b(x), x). \tag{3.23}
$$

Therefore, the gradient $\nabla_x J$ of the cost function can be obtained as the sum of the gradient of J with respect to x and the product of the gradient of J with respect to u and the gradient of u with respect to x. This product is necessary because the variable u depends on x through the PDE constraint. Hence,

$$
\nabla_x J = \frac{\partial J}{\partial x} + \frac{\partial J}{\partial u}\frac{\partial u}{\partial x}. \tag{3.24}
$$

It is necessary to evaluate how the gradient of u with respect to x is computed. Given that u is defined as $u = A^{-1}(x)b(x)$, the gradient can be computed as follows

$$\frac{\partial u}{\partial x} = \frac{\partial}{\partial x}(A^{-1}(x))b + A^{-1}(x)\frac{\partial bx}{\partial x}. \tag{3.25}$$

Applying the following propriety of the matrix:

$$A(x)A^{-1}(x) = I, \tag{3.26}$$

$$\frac{\partial}{\partial x}[A(x)]A^{-1}(x) + A(x)\frac{\partial}{\partial x}[A^{-1}(x)] = 0, \tag{3.27}$$

$$\frac{\partial}{\partial x}[A^{-1}(x)] = -A^{-1}(x)\frac{\partial}{\partial x}[A(x)]A^{-1}(x). \tag{3.28}$$

Finally, the gradient is obtained in the subsequent way as follows

$$\frac{\partial u}{\partial x} = -A^{-1}(x)\frac{\partial A(x)}{\partial x}A^{-1}(x)b(x) + A^{-1}(x)\frac{\partial b(x)}{\partial x} =$$
$$= A^{-1}(x)\left[-\frac{\partial A(x)}{\partial x}A^{-1}(x)b(x) + \frac{\partial b(x)}{\partial x}\right]. \tag{3.29}$$

By using this expression, it becomes feasible to calculate the gradient $\nabla_x J$, as

$$\nabla_x J = \frac{\partial J}{\partial x} + \frac{\partial J}{\partial u}A^{-1}(x)\left[-\frac{\partial A(x)}{\partial x}A^{-1}(x)b(x) + \frac{\partial b(x)}{\partial x}\right]. \tag{3.30}$$

It is worth noting that the term $A^{-1}(x)b(x)$ represents the definition of u, and in order to streamline the formulation, the term $\frac{\partial J}{\partial u}A^{-1}(x)$ will be defined equivalent to a new term called adjoint variable p, resulting in the following expression

$$\nabla_x J = \frac{\partial J}{\partial x} + p\left[-\frac{\partial A(x)}{\partial x}u + \frac{\partial b(x)}{\partial x}\right]. \tag{3.31}$$

Thus, in order to address this problem, two approaches are proposed. If we consider the term within the brackets in Equation 3.30 as a matrix, denoted as B, and $\frac{\partial J}{\partial u}$ as a vector v, we can obtain the product $A^{-1}B$ and then multiply it by v. It is important to note that the product $A^{-1}B$ is computed for each column of the matrix B, corresponding to each element x of the problem, as B depends on x. Furthermore, it is worth mentioning that A^{-1} is not explicitly computed due to its computational cost, but rather solved as a linear system of equations. However, due to the high computational cost associated with the first option, it is common to tackle this problem by employing the aforementioned variable p in Equation 3.31. By considering its definition as $p = vA^{-1}(x)$, the expression to be solved can be obtained:

$$A(x)p = \frac{\partial J}{\partial u}(x, u) \tag{3.32}$$

This is referred to as the adjoint problem since the computation of the gradient involves solving this additional system of equations. Subsequently, the algorithm for computing the gradient of the reduced cost will be presented.

1. Solve $A(x)u = b$ to find u.

2. Solve $A(x)p = \frac{\partial J}{\partial u}(x, u)$ to find p. It is important to note that in this step, u refers to the previous value of u, rather than the updated value computed in step 1.

3. Compute $\nabla_x J = \frac{\partial J}{\partial x} + p\left[-\frac{\partial A(x)}{\partial x}u + \frac{\partial b(x)}{\partial x}\right]$ with the updated values of u and p.

4. By employing a gradient descent method, the variable x is updated iteratively using the computed gradient according to the expression $x_{k+1} = x_k - t\nabla_x J$, where t is a scalar parameter called line search, chosen such that the reduced cost is minimized compared to the previous value of x. This condition is mathematically expressed as $J(x_k - t\nabla_x J) < J(x_k)$.

In the context of the elasticity problem, the adjoint problem can be interpreted as an additional displacement field that is determined by the gradient of J with respect to u, rather than being influenced by the applied force, represented by b, thus defining a self adjoint case in minimum compliance problems.

3.5 Unconstrained and constrained optimization problems

The interpretation of the adjoint problem as a Lagrange multiplier is also of considerable interest. In order to elucidate this concept, it is essential to grasp the fundamental concepts of unconstrained and constrained optimization problems.

In the case of an unconstrained optimization problem, the requisite condition for optimality to be satisfied is given by $\nabla J(x^*) = 0$. Note that when x is an element of $\mathbb{R}^n$, the optimality condition $\nabla J(x^*) = 0$ also belongs to $\mathbb{R}^n$. Consequently, in the case of having 10 unknowns, a system of 10 equations needs to be solved. On the contrary, in the case of a constrained optimization problem, the task of finding the optimal solution extends beyond solving the optimality condition $\nabla J(x^*) = 0$. It needs the fulfillment of additional conditions, namely $h(x) = 0$, which significantly increase the number of equations that must be addressed and the problem can not be solved. Therefore, it becomes necessary to employ Lagrange multipliers, denoted as λ, in order to handle such constraints. The number of Lagrange multipliers required corresponds to the number of constraints in the problem.

In this context, the functional Lagrangian is introduced. It is characterized as a scalar function due to the inherent scalar nature of $J(x)$, while the term $\lambda h(x)$ involves the multiplication of a vector by a transposed, resulting in a scalar value. Specifically,

$$L(x, \lambda) = J(x) + \lambda h(x). \tag{3.33}$$

Thus, when dealing with a formulated constrained optimization problem, the objective is to minimize the Lagrangian with respect to its variables. This in mathematical formulation can be expressed as follows:

$$D(\lambda) = \min_{x} \ L(x, \lambda) = \min_{x} \ J(x) + \lambda h(x), \tag{3.34}$$

where D is refered as the dual function.

Hence, the problem entails resolving the minimization of a combination of the objective function and the constraints, where the value of the Lagrange multiplier λ determines the influence of the constraints on the minimization problem. For example, in the scenario where the value of λ is either 0 or exceptionally low, the primary objective becomes the minimization of $f(x)$ but the constraint may not reach its minimum value so, the problem is not fully solved. Conversely, when λ assumes high values, the emphasis shifts to minimizing the constraint to 0, while the significance of $f(x)$ diminishes and the results are not optimal. Therefore, it can be demonstrated that the optimality condition translates into the maximization of $D(\lambda)$ since it is concave. Thus,

$$max \ D(\lambda) = \max_{\lambda} \min_{x} \ J(x) + \lambda h(x). \tag{3.35}$$

This is due to the fact that the minimization of the Lagrangian is aimed at the highest value of λ among all possible values. By minimizing the Lagrangian for this maximum value, the optimization is effectively carried out for all smaller values as well and the most optimal solution is obtained as it represents a balance between minimizing the constraint at its maximum point and simultaneously minimizing the objective function $J(x)$. This approach ensures the attainment of a highly competitive value that satisfies both criteria of the optimization problem.

The significance of $D(\lambda)$ is also worth commenting. It can be construed as a parameterized representation encompassing the minimum values of both the objective function and a part of the constraint influenced by the parameter λ. Hence, the resolution of the problem needs the determination of the maximum value of $D(\lambda)$.

Note that for a constrained optimization problem, the optimality conditions can be stated as the following

$$\frac{\partial L}{\partial x} = \frac{\partial J}{\partial x} + \lambda \frac{\partial h}{\partial x} = 0,$$
$$\frac{\partial L}{\partial \lambda} = h(x) = 0, \tag{3.36}$$

which system is known as the Karush-Kuhn-Tucker (KKT) conditions.

The derivative of L with respect to x is commonly referred to as the primal optimality condition, while the derivative of L with respect to λ is denoted as the dual optimality condition.

By introducing an additional optimality condition, the process required to solve the problem becomes more complex. However, it is important to emphasize that the increased number of constraints and unknowns is

accompanied by a corresponding increase in the number of equations. As a result, despite the augmented complexity, the problem remains solvable.

Moreover, by introducing the Lagrange multiplier, we can resume the aforementioned problem and provide an interpretation of the variable p as a Lagrange multiplier. Consequently, the initial problem can be formulated as the task of minimizing the sum of the cost function and the constraint multiplied by the Lagrange multiplier p as

$$\max_{p} \min_{x,u} \ L(x,u,p) = \max_{p} \min_{x,u} \ J(x,u) + p^T [A(x)u - b(x)]. \tag{3.37}$$

Here, the Karush-Kuhn-Tucker (KKT) conditions serve as a powerful tool also for resolving the adjoint problem in topology optimization. These conditions encompass the essential prerequisites for attaining optimality by incorporating the objective function, constraints, and design variables into the framework. In this particular context, the KKT conditions entail deriving the Lagrangian function with respect to each variable, namely p, u, and x as follows

$$\partial_p L(x,u,p) = A(x)u - b(x) = 0, \tag{3.38}$$

$$\partial_u L(x,u,p) = \frac{\partial J}{\partial u} + p^T A(x) = 0, \tag{3.39}$$

$$\partial_x L(x,u,p) = \frac{\partial J}{\partial x} + p^T \left[-\frac{\partial A(x)}{\partial x}u + \frac{\partial b(x)}{\partial x} \right]. \tag{3.40}$$

Having established this formulation, the variables u and p are determined with the the first and second conditions, respectively, as fixed points, meaning solving the system of equations. On the contrary, the variable x is computed through a gradient-based method. Consequently, to address the problem, it becomes necessary to compute the gradient, which, in turn, requires solving the aforementioned two systems of equations due to the presence of a PDE constraint. To this end, the following algorithm presents a potential approach for solving the problem:

1. Solve $A(x)u = b$ to find u.

2. Solve $A(x)p = \frac{\partial J}{\partial u}$ to find p.

3. Compute $\partial_x L = \frac{\partial J}{\partial x} + p^T \left[-\frac{\partial A(x)}{\partial x}u + \frac{\partial b(x)}{\partial x} \right]$ with the calculated values of u and p.

4. By employing a gradient descent method, the variable x is updated iteratively using the computed gradient according to the expression $x_{k+1} = x_k - t\nabla_x L$ (the parameter t, as introduced previously, maintains its original definition and usage in this steps of the algorithm). Lastly, the criterion to satisfy is expressed now as $L(x_k - t\nabla_x L, u, p) \ < \ L(x_k, u, p)$

It is noteworthy to emphasize that the optimizer is unaware of the variables u and p since they are obtained by solving the systems of equations and only required for the gradient computation. Thus, from the optimizer's

perspective, only the gradient is considered as information for the optimization process. For instance, in the specific case of a stress minimization problem, the variable p serves as a measure of the significance of equilibrium within the problem. In regions where p takes on higher values, the role of equilibrium becomes more pronounced and influential.

Steepest descent method as main basis for any solver.

If the problem is an unconstrained optimization problem, it can be effectively solved by employing a gradient-based method such as the steepest descent method. The gradient serves as a reliable indicator of the direction in which the objective function exhibits the steepest descent locally. By appropriately adjusting the step size, as determined by the line search parameter t, a descent is ensured. The steepest descent method can be mathematically formulated as follows:

$$x_{k+1} = x_k - t\nabla J(x_k). \tag{3.41}$$

The choice of t should be an appropriate value that strikes a balance between ensuring a descent in the optimization process and achieving computational efficiency. The chosen value should be small enough to guarantee the desired direction of descent while being large enough to expedite the algorithm's convergence.

It is worth noting the importance of devising an effective strategy for determining the value of t and for this reason substantial research efforts are being dedicated nowadays to the development of optimal line search techniques.

There is a particular case of a unconstrained optimization problem when a box constraint is imposed, demanding an alternative approach for its resolution, as presented below

$$\begin{aligned} \min_{x} \quad & J(x), \qquad x \in \mathbb{R}^n \\ \text{s.t.} \quad & 0 \leq x \leq 1 \end{aligned} \tag{3.42}$$

In the given context, the optimality conditions can be expressed as follows:

$$\nabla J(x^*) > 0 \quad x = 1, \tag{3.43}$$

$$\nabla J(x^*) = 0 \quad 0 \leq x \leq 1, \tag{3.44}$$

$$\nabla J(x^*) < 0 \quad x = 0. \tag{3.45}$$

These problems are approached by employing the method of alternating directions, as it takes into consideration the minimization of the cost function and the satisfaction of the constraints simultaneously.

The minimization process is tackled using the steepest descent method as mentioned earlier, while the constraint is handled through a process known as box projection:

$$\text{Box projection} \quad x_{k+1} = \ max \ (0, \ min \ (1, x_{k+1})). \tag{3.46}$$

The line search parameter t in the steepest descent method must satisfy two requirements: the projection of the volume and the descent of the direction.

To acquire additional insights into constrained problems and the dual problem in topology optimization, readers may refer to Appendix A for comprehensive information.

3.6 Optimization methods

In the context of unconstrained optimization problems, it is common to employ the following optimizers based purely in the steepest descent method:

- Project gradient. Specifically designed for density-based optimization problems ($x = \rho$).

- The Slerp optimizer. Applicable when working with Level Set topological optimization ($x = \Psi$).

- The Hamilton-Jacobi optimizer. Another approach for Level Set shape optimization problems ($x = \Psi$).

These optimizers primarily focus on updating the values of variable x. However, when dealing with constrained optimization problems, the following optimizers are commonly employed:

- Dual Nested in Primal. Can work with density and Level Set.

- Alternating Dual and Primal. Can work with density and Level Set.

- MMA (ρ), IPOPT(ρ)

- Fmincon (ρ)

- Null Space (ρ, Ψ)

- Etc.

These optimizers are specifically designed to handle optimization problems with constraints updating both the variables x and λ. It is noteworthy that the optimizers, namely Dual Nested in Primal, Augmented Lagrangian, and Null Space, are composed of unconstrained optimizers, as a constrained optimization problem always provides a means to update the variables x. Subsequently, a more comprehensive account for select optimizers that were previously introduced will be elucidated.

Projected gradient

In the case of the projected gradient method, a brief introduction has been provided earlier in relation to the steepest descent method using the following formulation

$$
\begin{aligned}
\min_{\rho} \; & J(\rho) \\
& \rho \qquad\qquad \rightarrow \qquad \min_{\rho} \; J(\rho) + \delta_{[0,1]}(\rho),
\\
& 0 \le \rho \le 1
\end{aligned}
\tag{3.47}
$$

which steps are

$$
\rho_{k+1} = \rho_k - t \nabla J(\rho_k),
\tag{3.48}
$$

$$
\text{Box projection} \quad \rho_{k+1} = \; max \; (0, \; min \; (1, \rho_{k+1})).
\tag{3.49}
$$

The approach aims to minimize both the box constraint $\delta_{[0,1]}(\rho)$ and the cost function $f(\rho)$ using a technique called alternating directions. This method involves two steps: first, minimizing the cost function while disregarding the constraint using the first equation mentioned; and second, finding the minimum value of the constraint while ensuring that it remains within the box using the second equation provided. It is important to note that the projected gradient method is applicable only to density optimization problems.

Slerp (Level Set)

On the contrary, in the context of level set optimization, the slerp optimizer is commonly employed as an effective approach. The slerp optimizer is characterized by the following formulation

$$
\begin{aligned}
\min \; & J(\Psi) \qquad ; \qquad && D_T J(\chi) < \; 0 \rightarrow \chi \; = \; 1 \\
& \Psi && D_T J(\chi) > \; 0 \rightarrow \chi \; = \; 0 \;,
\end{aligned}
\tag{3.50}
$$

$$
J_1(\chi + \Delta\chi) = J_0(\chi) + D_T J(\chi)\Delta\chi.
\tag{3.51}
$$

This optimizer uses the topological derivative to assess the impact of introducing a hole in the structure on the cost function. By introducing a small perturbation in the structure, this formulation allows for the evaluation of how the cost (such as compliance) would change. Consequently, the formulation expresses the cost variation as a linear combination. Considering the characteristic function's requirement to take values of 1 or 0, the topological derivative must be negative or positive, respectively.

It is worth remembering that in order to achieve optimality, the Level Set formulation should exhibit the same sign as the topological derivative. Specifically, when the characteristic function χ takes a value of 1, the Level Set should have a negative sign, while a value of 0 for χ should correspond to a positive sign. Consequently, the optimality condition can be established as $D_T J(\chi) = \Psi$, up to a constant, while ensuring that the signs remain consistent. To solve these optimization problems, the following formula is commonly employed

$$\Psi_{k+1} = \alpha_k(\kappa)\Psi_k + \beta_k(\kappa)D_T J(\chi(\Psi)). \tag{3.52}$$

The values of α_k and β_k are determined to satisfy $||\Psi_{k+1}|| = 1$, while the convergence criterion θ requires the scalar product of the Level Set and the topological derivative to be minimized.

Alternating primal and dual

For a constrained optimization problem, the objective is to minimize the specified objective function within the bounds defined by the given constraints. Consider the following constrained problem

$$\begin{aligned} &\min_{x} && J(x) \\ &\text{s.t} && h(x) = 0 \end{aligned}. \tag{3.53}$$

In the preceding sections, the Karush-Kuhn-Tucker (KKT) conditions for a basic constrained optimization problem have been expounded upon. For a basic constrained optimization problem the KKT are the following:

$$\left.\begin{aligned} \nabla J + \lambda \nabla h \\ h(x) = 0 \end{aligned}\right\} = KKT. \tag{3.54}$$

One approach to tackle the optimization problem is by formulating a linear penalization problem, where λ_k is introduced as an additional unknown. It is important to note that despite this formulation, the problem still retains its constraints as

$$\begin{aligned} &\min_{x} && J(x) + \lambda_k h(x) \\ &\text{s.t} && h(x) = 0 \end{aligned}, \tag{3.55}$$

$$\left.\begin{aligned} \nabla f + (\lambda + \lambda_k)\nabla C = 0 \\ C(x) = 0 \end{aligned}\right\} = KKT. \tag{3.56}$$

The introduced unknown can subsequently be eliminated through a quadratic penalization approach, removing the variable via a quadratic penalty. In contrast to the linear penalization, this formulation does not impose any constraints as shown

$$min_x \ J(x) + \frac{1}{2}\rho \ h(x)^2, \tag{3.57}$$

$$KKT = J(x) + (\rho h)\nabla h = 0. \tag{3.58}$$

By combining these two procedures, introducing an unknown variable through linear penalization and eliminating an unknown variable by incorporating a constraint in the cost function using quadratic penalization, the augmented Lagrangian method is obtained. It is noteworthy that the original constrained problem has been transformed into an unconstrained problem through the addition of an unknown variable. The final constrained problem yields

$$min_x \ J(x) + \lambda_k h(x) + \frac{1}{2}\rho \ h(x)^2, \tag{3.59}$$

$$KKT = J(x) + (\lambda_k + \rho h)\nabla h = 0 \tag{3.60}$$

Despite the transformation of the problem, the underlying concept remains the same, aiming to determine λ_k such that it converges to λ. This solving approach is referred to as the augmented Lagrangian method, as the primary objective is to minimize the Lagrangian (consisting of the first two terms of the formulation above) in addition to a penalty term (the last term of the formulation) determined by the parameter c, known as the penalty parameter.

Therefore, the augmented Lagrangian is formulated as follows for updating the variable x and solving the problem

$$L_A(x, \lambda_k) = J(x) + \lambda_k h(x) + \frac{1}{2}\rho \ h(x)^2, \tag{3.61}$$

$$max_\lambda \ min_x \ L_A(x, \lambda), \tag{3.62}$$

$$\left.\begin{array}{l} x_{k+1} = x_k - \alpha\nabla L_A(x, \lambda_k) \\ \lambda_{k+1} = \lambda_k + \rho \ C(x_k) \end{array}\right\}, \tag{3.63}$$

where L_A represents the definition of the augmented Lagrangian. This method of problem resolution is commonly referred to as alternating primal and dual, as it involves alternating between two steps: updating the variable x and updating the Lagrange multiplier λ. The objective is to find a suitable value for α such that $L_A(x_{k+1}, \lambda_k) < L_A(x, \lambda_k)$. If this condition is not satisfied, t is divided by two. Finally, the new value of λ is computed based on the updated variables and Lagrangian.

Dual Nested in Primal

In this case, the mathematical formulation can be expressed as follows:

$$\begin{aligned} &\min_{x} && J(x) \\ &\text{s.t} && h(x) = 0 \end{aligned} \tag{3.64}$$

$$x_{k+1} = x_k - t\nabla L(x, \lambda_k) \tag{3.65}$$

$$h(x_{k+1}) = 0 \tag{3.66}$$

The objective in this case, in contrast to previous methods, is to find suitable values for t and λ such that $L(x_{k+1}, \lambda_k) < L(x, \lambda_k)$. Subsequently, the volume is modified and assessed to ensure it fulfills the constraint. If the constraint is not satisfied, the value of λ is recomputed, and this iterative process is continued. This approach is referred to as "dual nested in primal" because the constraint is always satisfied, and there is no alternating process as in previous methods.

Null Space

The null space optimizer operates by decomposing the design variables gradient flow into two components: the null space component and the active constraint component. The null space component represents the part of the design that can be freely manipulated without violating any constraints, while the active constraint component ensures that the design adheres to the imposed constraints. By optimizing the null space component independently, the optimizer can explore different design configurations and identify solutions that may have been overlooked in traditional optimization approaches. Further information regarding the functioning of this optimizer is expounded upon in the subsequent section. It is noteworthy to acknowledge the work in literature as a valuable source for in-depth insights and comprehensive understanding of the Null Space optimizer [45].

In this case the mathematical formulation is expressed by the following expressions

$$\begin{aligned} &\min_{x} && J(x) \\ &\text{s.t} && h(x) = 0 \end{aligned}, \tag{3.67}$$

which can be also expressed as

$$\min_{x} \max_{\lambda} \ J(x) + \lambda \, h(x). \tag{3.68}$$

The mathematical formulation involves employing a quadratic expansion of the Lagrangian. Subsequently, it can be proved that the technique of alternating directions is implemented in the following manner:

$$\text{For } (\lambda, x) : \begin{cases} \lambda_k = A_G (\nabla h^T \nabla h)^{-1} \cdot h - A_J (\nabla h^T \nabla h)^{-1} \nabla h \nabla J \\ x_{k+1} = x_k - t(\nabla J + \lambda_k \nabla h) \end{cases}, \tag{3.69}$$

After each iteration, the quadratic expression for the Lagrangian is updated with the new design variable distribution ($x_k = x_{k+1}$).

Then, the process consists in iterate until it is fulfilled that $||L(x_{k+1}) - L(x_k)|| < \delta$.

Chapter 4

Numerical study

In this section, Topology Optimization methods will be employed for the design of two compliant mechanisms. The design process will be conducted using Finite Element Methods (FEM) through the implementation of the Swan code. Swan is a specialized Topology Optimization software developed in Matlab, facilitating the resolution of 2D and 3D topology optimization problems using density or level-set variables as design parameters. The numerical methodology applied in the designs will incorporate both density-based SIMP and Level Set methods.

4.1 Design of compliant mechanism with topology optimization methods

The finite element method is a numerical technique for solving problems which are described by partial differential equations or can be formulated as functional minimization. A domain of interest is represented as an assembly of finite elements [46]. The design process of compliant mechanisms in topology optimization necessitates the utilization of FEM, whereby the topology optimization problem is implemented within a discretized domain.

The initial phase in the design process of compliant mechanisms entails identifying the specific domain for each intended design to be developed. Within the scope of this paper, two distinct designs will be undertaken: the compliant force inverter and the gripper mechanism seen in state-of-the-art for the application in [31], for instance.

Recall that a gripper mechanism converts a force, applied at the input port, into an output displacement at the two output ports in an orthogonal direction to the force vector. On the other hand, an inverter is a mechanism that converts an input force applied at the input port, into an opposite output displacement at the output port [47].

4.1.1 Design of a gripper mechanism

With the purpose of implementing the acquired knowledge in topology optimization, the present part aims to determine the optimal design of a gripper mechanism. To achieve this objective, the computational domain illustrated in Figure 4.1 is discretized into a quadratic mesh comprising a total of 20.000 elements.
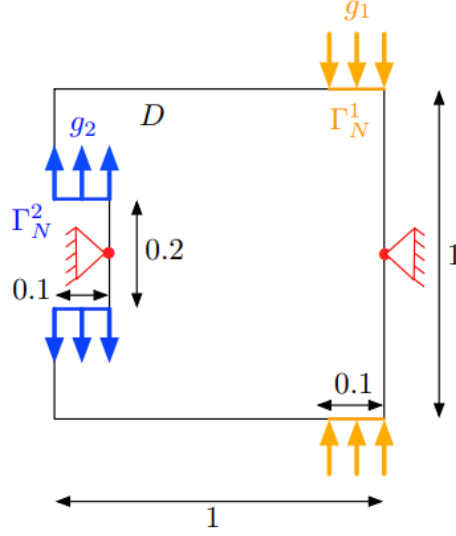
Figure 4.1: Setting of the gripping mechanism. Extracted from [48].

The structure is fixed at two nodes on its symmetry axis; the region Γ_N where loads are applied is decomposed as $\Gamma_N = \Gamma_N^1 \cup \Gamma_N^2$ and :

- Vertical loads $g_1 = (0, \pm 10)$ are applied on Γ_N^1, which represent the pressure exerted by the user,

- Vertical loads $g_2 = (0, \pm 1)$ are applied on Γ_N^2, which account for the reaction force applied by the object undergoing the action of the gripping mechanism.

The considered objective function $J(\Omega)$ reads:

$$J(\Omega) = \int_{\Gamma_N} k \cdot u_\Omega \, ds + \text{Vol}(\Omega),$$

where the vector k is defined by:

- $k = (0, -1)$ on the upper side of Γ_N^1 and $k = (0, 1)$ on the lower side of Γ_N^1,

- $k = (0, 2)$ on the upper side of Γ_N^2 and $k = (0, -2)$ on the lower side of Γ_N^2,

so that it is expected that the elastic displacement of the resulting design shows a pinching of the jaws Γ_{2N} without inducing an excessive displacement of the region Γ_{1N} where the user applies forces [48].

In this particular case, the topology optimization (TO) problem can be mathematically formulated as follows

$$\begin{aligned} \min_{\chi} \quad & J(\Omega) \; , \\ \text{s.t} \quad & V(\Omega) - V^* \leq 0 \; . \end{aligned} \tag{4.1}$$

It is worth noting that the problem under consideration is not self-adjoint, in contrast with minimum compliance case.

The computational domain has been constructed utilizing the GID software, a comprehensive CAD system that features the widely used NURBS surfaces for the geometry definition, including several CAD repairing tools and mesh generators. The applied conditions and the delineated domain are visually represented in Figure 4.2.
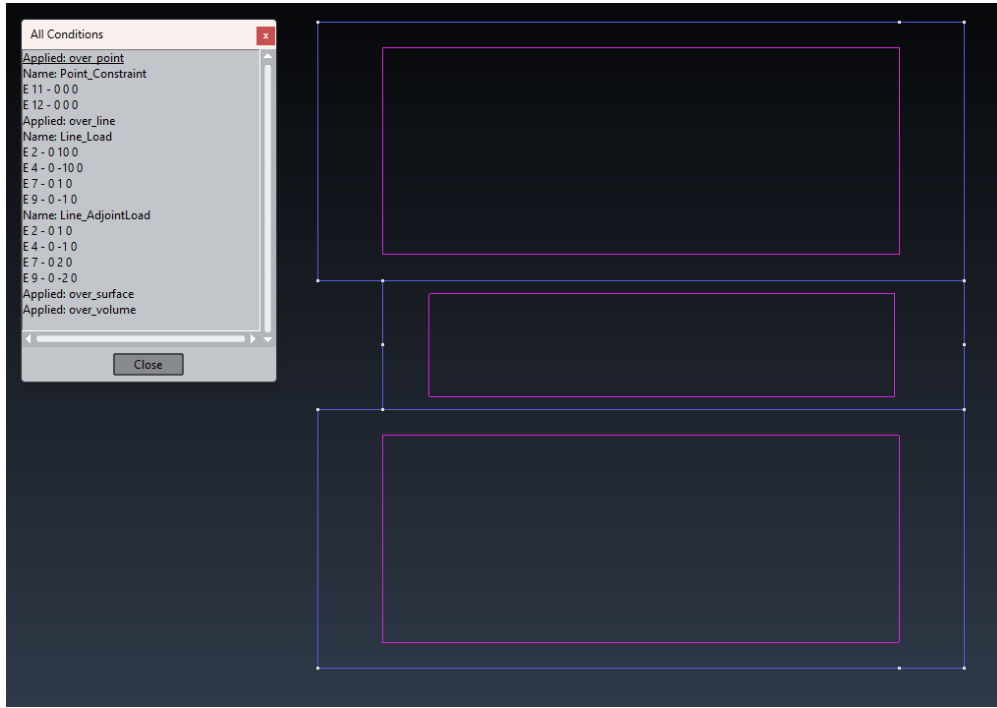
Figure 4.2: Gripper mechanism domain with the applied conditions.

The mesh, as depicted in Figure 4.3, has been also generated and computed employing GID software and is used for the computation in the Swan code, employing the "Null Space" optimizer in conjunction with the "Projected Gradient" Primal Updater for the Density design variable, and "SLERP" for the Level Set design variable. Computations have been performed for volume fractions of 0.5, 0.4, 0.3, and 0.2, individually for each design variable.
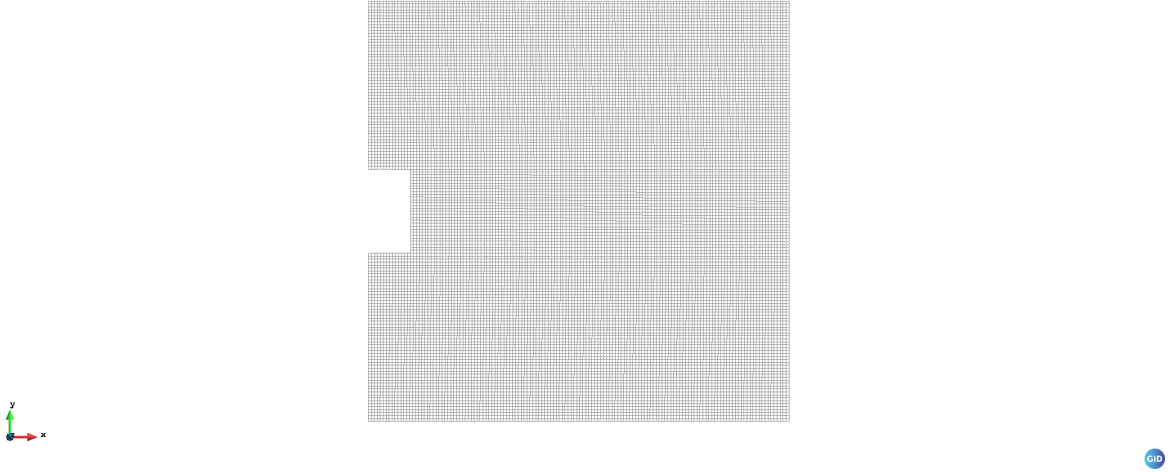
Figure 4.3: Gripper mechanism mesh.

The ensuing code snippet illustrates the pertinent segment wherein the conditions are explicitly defined.

```
1  filename = 'gripping'; % Try other meshes
2  ptype = 'MACRO';
3  method = 'SIMPALL';
4  materialType = 'ISOTROPIC';
5  initial_case = 'full';
6  cost = {'nonadjoint_compliance'};
7  weights = [1];
8  constraint = {'volumeConstraint'};
9  incrementFactor = 1.2;
10 optimizerUnconstrained = 'PROJECTED GRADIENT'; % See PrimalUpdaterFactory
11 optimizer = 'NullSpace'; % See OptimizerFactory
12 designVariable = 'Density'; % Density/LevelSet
13 filterType = 'P1';
14 constraint_case = {'INEQUALITY'}; % EQUALITY or INEQUALITY
```

The variable indicated in line 2 of the code signifies the type of problem, which can be toggled between MACRO and MICRO. The former is employed for structural problems, while the latter pertains to representative volumes of a domain. In this particular study, the MACRO problem type is utilized, as the objective is to design structures. Furthermore, the 'SIMPALL' method assigned to the 'method' variable dictates the interpolation approach for density.

It is important to note that this thesis solely focuses on topology optimization (TO) problems where the cost function is non-adjoint, accompanied by a volume constraint. Other types of TO problems are intentionally omitted from the scope of this research. These specific constraints are defined in lines 6 and 8 of the code.

Within the framework of employing the Null Space optimizer, it is essential to define and specify two pivotal functions, namely 'aJmax' and 'aGmax' empowering the Lagrange multipliers concerning the Nullspace and range space directions, respectively. . Additionally, gaining a comprehensive understanding of the functioning of the Null Space optimizer is of interest. The Null Space optimizer initiates the optimization process from a random initial point and proceeds by traversing two distinct directions, with the objective of simultaneously minimizing the cost and adhering to the imposed constraints. The 'aJmax' function denotes the direction that facilitates the reduction of the variable, while 'aGmax' represents the direction that guides the optimization towards satisfying the constraints.

It is worth noting that if these variables are set to zero in the code, the simulation ceases to progress, as it results in the nullification of the Lagrange multiplier. As a consequence of the monotonic behavior of the compliance function, the volume remains unaltered in such cases. Thus, comprehending this concept in depth is of paramount importance. In Figure 4.4, a visual depiction illustrating the operational concept of the Null Space optimizer is presented.
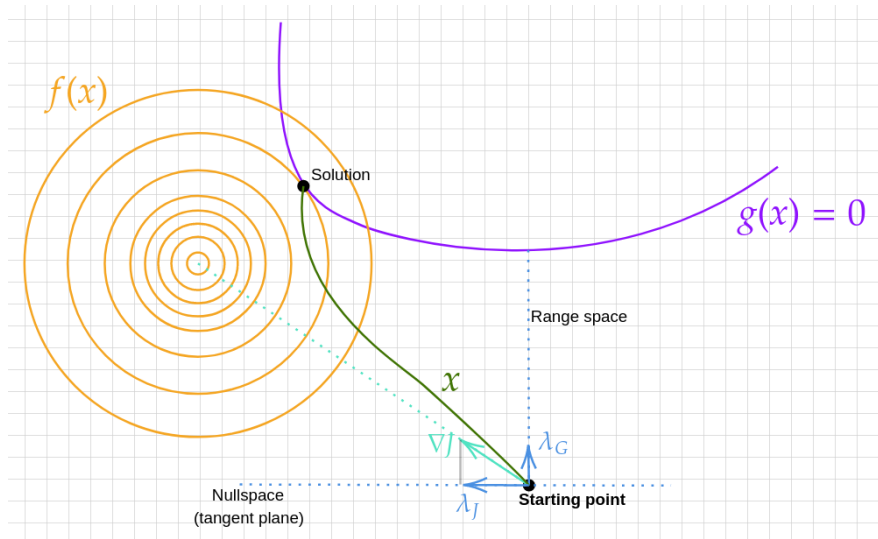
Figure 4.4: Visual representation of the operational concept of the Null Space optimizer.

The strategy for determining the values of aJ and aG entails an initial focus on gradually approaching the desired J value until achieving a stable volume in close proximity to the target volume. Finding the optimal balance between a large J value, which may yield a feasible solution but not necessarily the optimal one, and a small J value, which may fall short of achieving the desired final volume, is of paramount importance. Once a satisfactory J value is achieved, the estimation of G becomes the subsequent objective.

To estimate the G value, the code segment corresponding to the Lagrange multiplier associated with G, which is located in the DualUpdater_NullSpace class, is utilized. The Lagrange multiplier can be decomposed into two parts: the part associated with G and the part associated with J, both of which are the values under investigation. The λ_J values typically range from 1 to 9, or on the order of 10^0. Similarly, the λ_G value needs to be within the same order of magnitude to maintain balance in the problem.

Consequently, it can be checked that the assigned value for 'aGmax' should be on the order of 10^{-1} or 10^{-2} to achieve this balance in accordance with its mathematical formulation.

For the design of the gripper mechanism, a total of eight simulations have been performed, each requiring a search for different values of 'aJmax' and 'aGmax'. The final values for these two variables in each simulation are presented in Table 4.1.

Table 4.1: Final values used in the gripping mechanism simulations for 'aJmax and 'aGmax' variables.

Volume Fraction	Density		Level Set	
	aJmax	aGmax	aJmax	aGmax
0.5	2.3	0.3	0.1	0.3
0.4	2	0.3	0.1	0.1
0.3	0.5	0.3	0.3	0.1
0.2	0.1	0.01	0.1	0.01
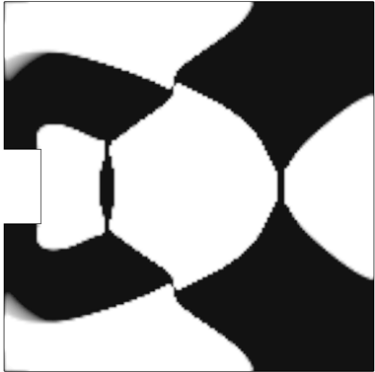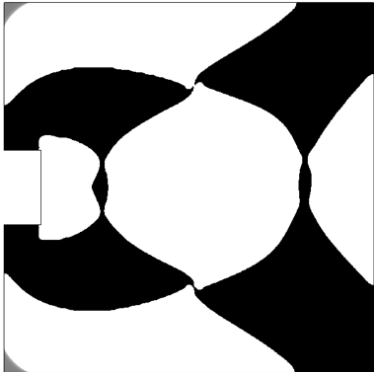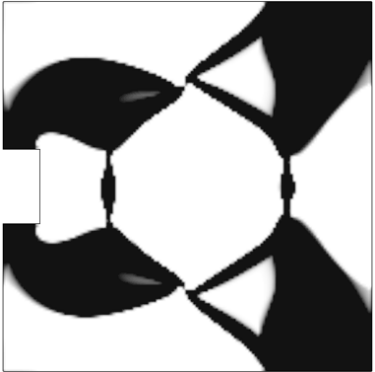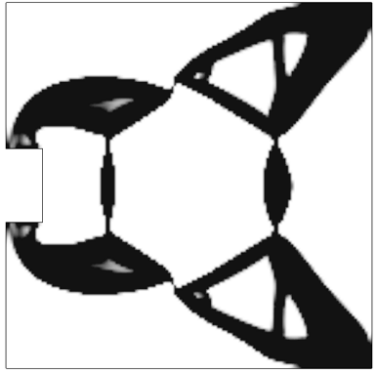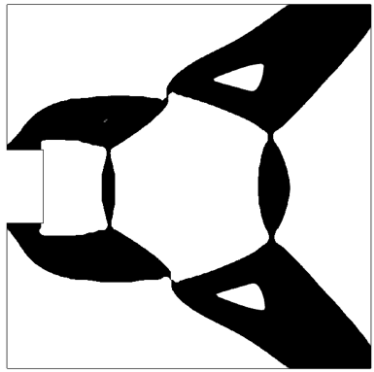
Finally, the results of the gripping mechanism simulation are presented in Table 4.2. The code was configured to execute 1000 iterations, starting from an initial volume value of 1.

It is worth mentioning that the results obtained from the Matlab code have been post-processed using the GID software. For the design variable Density, a minimum display value of 0 and a maximum display value of 1 were set. Similarly, for the design variable Level Set, a minimum display value of -0.001 and a maximum display value of 0.001 were applied.

Based on the obtained results, several conclusions can be drawn. Firstly, it is observed that both the density and level set methods yield similar outcomes for equivalent volumes. Additionally, it is noteworthy that the density optimizer displays gray values in the results, indicating the utilization of a wider range of values between the two extremes. This phenomenon arises due to the inherent complexity of achieving outcomes solely restricted to the two prescribed values.

Upon examination of the calculated values from the code, it becomes evident that the structure does not initially exhibit characteristics of a CM. However, as the simulation progresses, the introduction of hinges leads to the transformation of the structure into a CM. This transition is reflected in the final stage of the simulation, where the cost function $J(\Omega)$ assumes a negative value, indicating a reversal in the achieved display of the mechanism u_{out}.

Table 4.2: Final results of the gripping mechanism simulations.

Volume Fraction	Density	Level Set
0.5		
0.4		
0.3		

It should be noted that as the volume decreases, the results exhibit an increased number of holes and hinges. This behavior can be attributed to the algorithm's attempt to satisfy the increasingly stringent volume constraint. As the algorithm strives to meet the specified volume requirement, it introduces additional voids and hinges in the structure. This observation highlights the trade-off between volume reduction and the complexity of the resulting design.

Finally, it is worth noting that while it was initially planned to conduct eight simulations for these mechanisms, the simulations for a volume fraction of 0.2, although feasible, yield a final result with a larger volume fraction than desired. This discrepancy becomes apparent when comparing the volume of the simulation conducted for a volume fraction of 0.2, as depicted in Figure 4.5, to the volume of the simulation conducted for a volume fraction of 0.3.
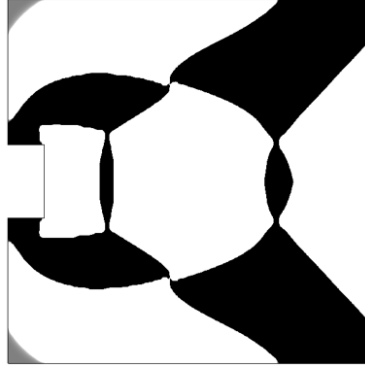
Figure 4.5: Simulation conducted for a volume fraction of 0.2 with level set optimizer.

In the appendix, an example of the gripping mechanism designed using the MMA optimizer can also be found. This example serves as a demonstration of the application of the MMA optimizer in generating an optimized gripping mechanism.

4.1.2 Design of an inverter mechanism

To introduce further diversity to the study, an alternative design is proposed. In this case, the computational domain is a 1x1 square discretized into 10,000 elements. Figure 4.6 illustrates a visual representation of the domain for an inverter mechanism design.
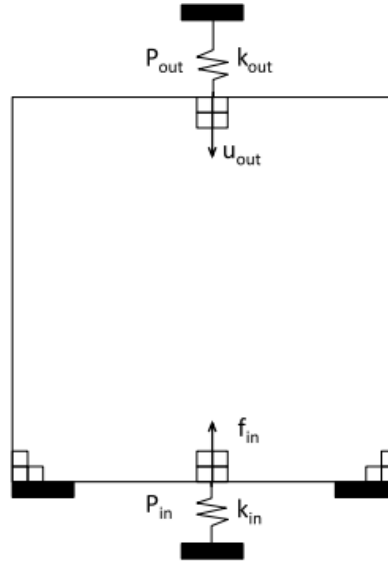
Figure 4.6: Design domain for an inverter mechanism. Extracted from [49].

The structure is fixed in two segments, spanning from the coordinates (0,0) to (0.1,0) and from (0.9,0) to (1,0) along the lower section. The loads are applied along the symmetry axis in both the lower and upper regions of the structure. The magnitudes of these loads are as follows:

- The structure is subjected to a concentrated input force, $f_{in} = 20N$, associated to a positive sign as shown in the vector of Figure 4.6.

- The adjoint load k is applied in the upper point, where the displacement of the structure is expected, and has a values of $k = 0.1$ associated to a positive sign. In the lower part of the structure the value of the adjoint load is omitted.

The expected direction of displacement for the mechanism is denoted as u_{out} and is indicated in Figure 4.6. It can be observed that u_{out} is oriented in the opposite direction to the applied force, thus fulfilling the intended function of an inverter mechanism.

The topology optimization problem is mathematically identical as the previous case, see Equation 4.1.

The computational domain utilized for the analysis has been generated using GID. The applied conditions and the defined domain are visually depicted in Figure 4.7.
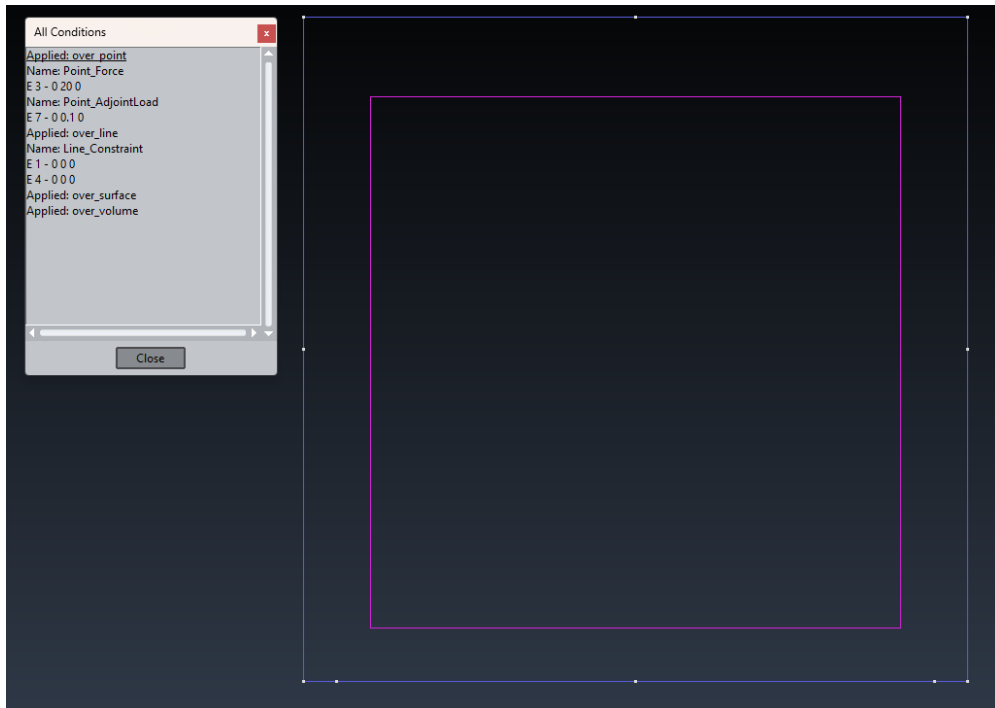
Figure 4.7: Inverter mechanism domain with the applied conditions.

The mesh, as depicted in Figure 4.8, has been also generated and computed employing GID software.
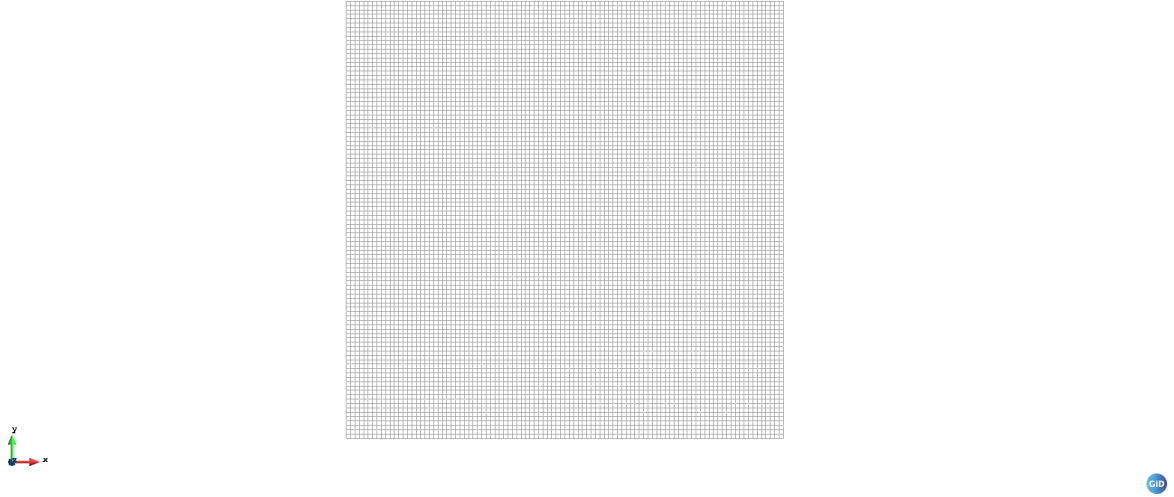
Figure 4.8: Inverter mechanism mesh.
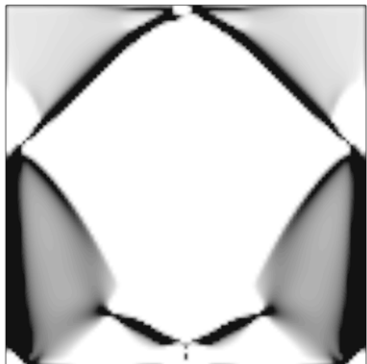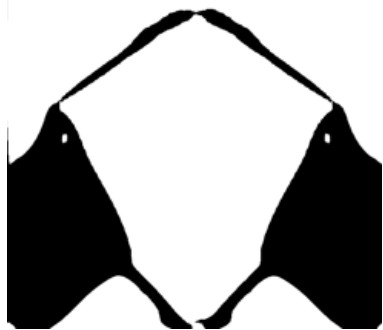
For the design of the inverter mechanism, a total of two simulations have been performed, each requiring a search for different values of 'aJmax' and 'aGmax'. The final values for these two variables in each simulation are presented in Table 4.3 .

Table 4.3: Final values used in the inverter mechanism simulations for 'aJmax and 'aGmax' variables.

Volume Fraction	Density		Level Set	
	aJmax	aGmax	aJmax	aGmax
0.3	8	3.5	2.5	2

Finally, the results of the inverter mechanism simulation are presented in Table 4.4. The code was configured to execute 1000 iterations, starting from an initial volume value of 1.

Table 4.4: Final results of the inverter mechanism simulations.

Volume Fraction	Density	Level Set
0.3		

Based on the results obtained for the inverter mechanisms, several conclusions can be drawn. Initially, it was planned to conduct eight simulations for these mechanisms, similar to the gripping mechanisms. However,

52

both the simulations and existing literature have revealed a significant challenge in studying higher volumes, such as 0.4 or 0.5. Figure 4.9 demonstrates that conducting a simulation for a volume fraction of 0.4 presents substantial difficulties in adjusting the parameters aG and aJ, resulting in inaccurate and infeasible outcomes.
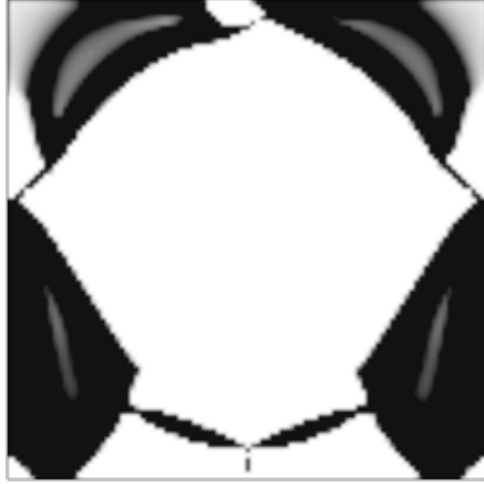
Figure 4.9: Inverter mechanism simulation for a 0.4 volume fraction.

In general, this design has posed greater difficulties, particularly in adjusting the values of the Null Space optimizer and conducting simulations for volume fractions other than 0.3. The results obtained for the Density design variable have posed a significant challenge in achieving outcomes without gray values, although both obtained results are considered satisfactory.

Chapter 5

Application example in aerospace

This section aims to provide a comprehensive exploration of the aerospace and aeronautic domain within the context of compliant mechanisms and topology optimization. In line with this objective, a specific implementation pertaining to the aeronautical field is proposed. By applying compliant mechanisms and topology optimization techniques, this study seeks to address and contribute to the unique challenges and requirements of the aerospace and aeronautic industry. Through this focused approach, the potential benefits in this field can be better understood.

5.1 Practical application in the aeronautical field: Variable geometry trailing edge flap

In the preceding sections, a comprehensive array of applications involving compliant mechanisms across various domains, with a particular emphasis on the aerospace field, has been presented. Nevertheless, there is a specific example that warrants further attention and will be thoroughly examined in this final chapter, owing to its profound significance in shaping novel aircraft designs.

Hence, the subsequent discussion will focus on the specific application of compliant mechanisms and topology optimization in the context of a variable geometry trailing edge flap.

The primary objective of incorporating the variable geometry trailing edge flap was to create a hingeless and continuous flap mechanism capable of effectively adjusting the wing's camber. This adjustment aimed to minimize drag across various lift conditions. In contrast to conventional flap deflection methods, which often result in flow separation and increased drag, the use of variable geometry compliant trailing edge flaps offers mission adaptive wing capabilities without imposing substantial penalties in terms of weight, space, or power requirements.

5.1.1 Design approach

Although this study does not involve the code developing of a compliant trailing edge flap design, it aims to propose preliminary design specifications for this application. The primary objective is to design a variable geometry trailing edge flap for a high altitude, long endurance air vehicle configuration. An important requirement for the design is the capability to achieve differential deflection along the wing span to optimize wing loading. The target shapes sought for the flap are those that exhibit the smoothest possible shape change while effectively achieving the desired deflection.

It is worth mentioning that in the literature, a design with similar specifications has been proposed [34]. Furthermore, regarding the design presented in Figure 5.1 the literature study builds upon the previous work by FlexSys Inc., which represents cutting-edge technology in the field of compliant trailing edge flap design [50].
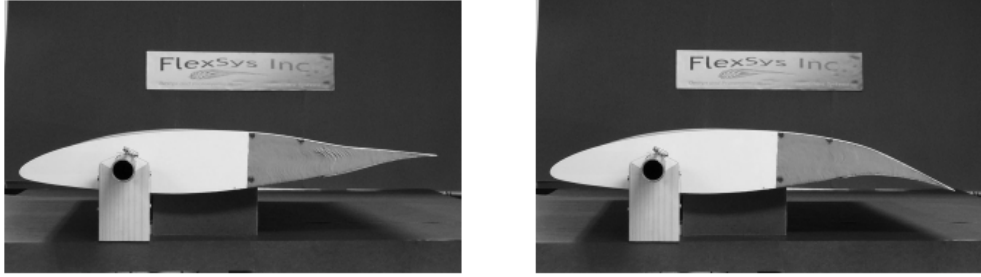
Figure 5.1: Variable geometry trailing edge wind tunnel model shown in -10 degrees and +10 degrees positions. Extracted from [34].

5.1.2 Aerodynamic benefits

Because endurance aircraft experience weight variations as much as 50% or more during a typical mission, minimizing wing drag over a wide lift range is critical for mission efficiency. The compliant variable geometry trailing edge flap provides a distinct performance advantage over a conventional trailing edge flap. This point is easily illustrated using experimental wind tunnel data. Figure 5.2 presents wind tunnel aerodynamic data for a typical modern high altitude long endurance airfoil with a conventional 20% chord trailing edge flap. The data shows conclusively that deflecting a conventional flap downward increases the airfoil lift coefficient; however, for the two positive flap deflections shown, airfoil drag is simultaneously increased. This drag rise is caused by flow separation in the pressure recovery region on the aft portion of the airfoil upper surface. This region of flow separation is induced by the sharp increase in radius of curvature on the airfoil upper surface as the conventional flap rotates downward [34].

Notice that airfoil drag performance is still acceptable when the trailing edge is deflected up. In this position there is a decrease in radius of curvature on the upper surface, and while deflecting the flap trailing edge up limits airfoil lift, the flow is still fully attached on both airfoil surfaces [34].
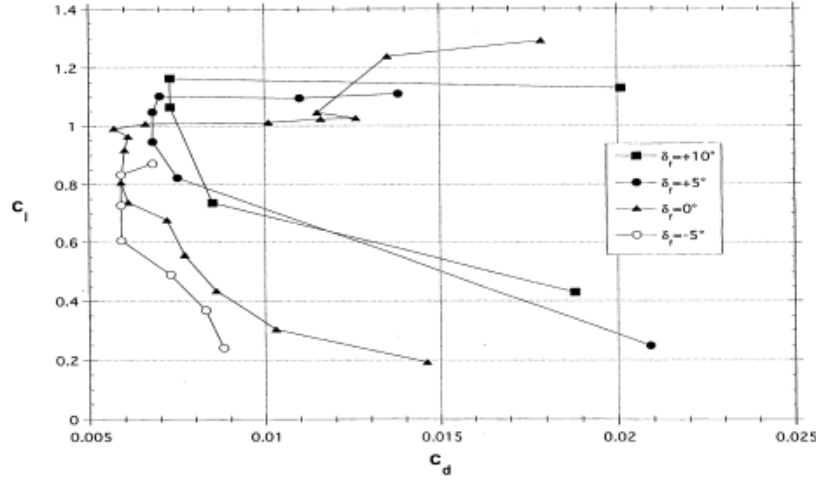
Figure 5.2: Cl vs. Cd data for a modern long endurance airfoil with a conventional trailing edge flap. Extracted from [34].

Data taken at the Ohio State University low speed wind tunnel is shown in Figure 5.3. Here, the adaptive compliant flap shows much better drag control than is possible with a conventional flap design. When a variable geometry compliant trailing edge flap is used, the process is such that the radius of curvature on the airfoil upper surface can be contoured for maximum flow attachment in the pressure recovery region. Notice that consistently low drag levels are maintained as the flap is deflected downward and the airfoil aft upper surface is continually reshaped during the deflection process. Comparing these results with those presented in Figure 5.2, and the aerodynamic advantage of using a variable geometry trailing edge for endurance aircraft applications becomes quite obvious. [34]
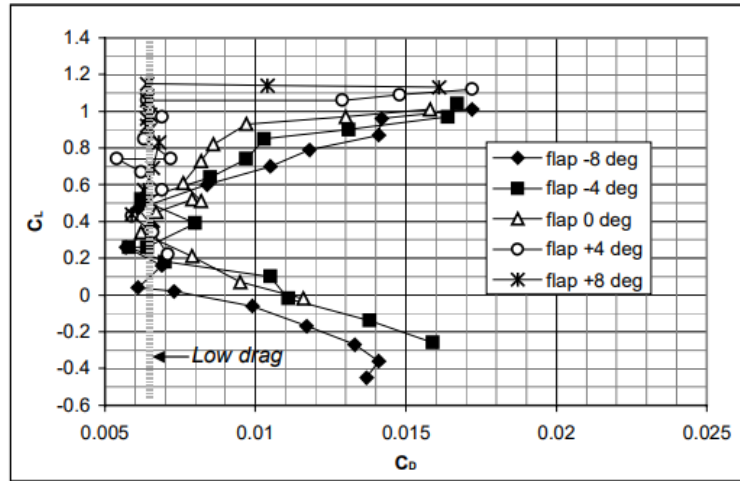
Figure 5.3: Wind Tunnel results highlight the benefits of FlexSys variable geometry trailing edge flap. As the flap angle is changed from -8 degrees to +8 degrees, the CL increases from 0.1 to 1.1 without increasing the drag. Note the low drag envelop (CD = 0.0065) during the entire excursion. Extracted from [34].

Therefore, based on the evident advantages of incorporating a compliant trailing edge flap, it can be concluded that topology optimization can be used in subsequent stages of the design process to identify an optimal shape that meets all the aforementioned requirements.

Chapter 6

Budget summary and economic feasibility study

The objective of this section is to provide an estimation of the overall hypothetical cost associated with the development of a project similar to the one presented in this paper.

The financial assessment of this project, which justifies its initial investment, encompasses several categories of expenses, namely Human Resources (Table 6.1), Software (Table 6.2), and other resource-related costs (Table 6.3). These components collectively contribute to the comprehensive financial structure of the project, ensuring sufficient allocation for personnel, requisite software applications, and other indispensable resources.

Table 6.1: Human Resources Plan

Human Resources Plan

ID	Description	Hours	Cost/u (€)	Total Cost (€)
1.1	**Project Management.** Costs relative to project development time.	600.00	20.00	12,000.00
			Total	**12,000.00 €**

Table 6.2: Operating Expenses

Operating Expenses

ID	Description	Cost (€)
2.1	**Permanent Licenses**	
2.1.1	Matlab & Simulink	2,000.00
2.1.2	GID Simulation	1,100.00
	Total	**3,100.00 €**

Table 6.3: Resources Costs

Resources Costs

ID	Description	Hours	Cost/u (€)	Cost (€)
3.1	**Overhead expenses**			
3.1.1	Computer		1,200.00	1,200.00
3.1.2	Office supplies		200.00	200.00
			Total	1,400.00 €
3.2	**Utilities expenses**			
3.2.1	Electricity	600.0	0.22	132.00
3.2.2	Internet	600.0	0.11	66.00
			Total	198.00 €
			Total Resources Costs	**1,598.00 €**

Finally, Table 6.4 presents the comprehensive budget, incorporating all the aforementioned expenses, along with the inclusion of contingency reserves. Contingency reserves serve as financial provisions that allow for flexibility and mitigate the risks associated with budget overruns. In this particular project, a contingency reserve of 10% of the total budget has been allocated, considering the nature of the project as a cutting-edge technology initiative that often encounters time delays.

Table 6.4: Project Total Budget

PROJECT TOTAL BUDGET

Human Resources Plan				
ID	Description	Hours	Cost/u (€)	Cost (€)
1.1	**Project Management.** Cost relative to project development time	600.0	20.00	12,000.00
			Total	12,000.00 €
Operating Expenses				
ID	Description		Cost/u (€)	Cost (€)
2.1	**Permanent Licenses**			
2.1.1	Matlab & Simulink		2,000.00	
2.1.2	GID Simulation		1,100.00	
			Total	3,100 €
Resources Costs				
ID	Description	Hours	Cost/u (€)	Cost (€)
3.1	**Overhead expenses**			
3.1.1	Computer		1,200.00	1,200.00

3.1.2	Office supplies		200.00	200.00
			Total	1,400.00 €
3.2	**Utilities expenses**			
3.2.1	Electricity	600.0	0.22	132.00
3.2.2	Internet	600.0	0.11	66.00
			Total	198.00 €
4.1	**Contingency Reserves**	Value considered: 10%	Total	1,669.80 €
			Total Costs	**18,367.80 €**

6.1   Schedule

The Clean Code Development task was conducted in combination with the last semester of the Bachelor's program starting in September 2022.

In addition, since February 2023, a weekly meeting with the tutor and co-tutor has been held every Tuesday to discuss the previous week's work and set goals for the upcoming week. From February until now, the literature review has been conducted. During the above meetings, the information and the working of the CMs found during the week are explained.

Since March, the study on topology optimization concepts has been done. The goal for the next few weeks is to start working on the code provided by the tutor and continue searching for literature and CMs of interest. Finally, a Gantt chart is provided below with an approximate timeline of goals and tasks to be completed.
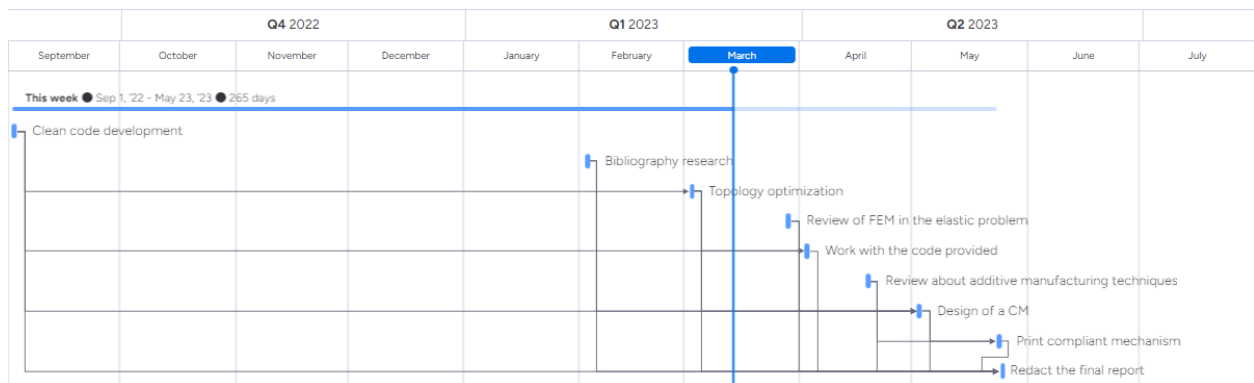
Chapter 7

Analysis and assessment of environmental implications

In this section, the environmental implications associated with the implementation of the mechanisms investigated in this study within engineering projects will be examined. The principal focus will be on analyzing the specific case of flexible trailing edge flaps and their potential contribution to fuel reduction in aviation.

Flexible trailing edge flaps (FTEFs) have emerged as a promising technology in the aviation industry, offering significant fuel efficiency benefits compared to traditional deflecting flaps. By seamlessly modifying the shape of the wing's trailing edge, FTEFs provide enhanced control over lift and drag, resulting in reduced fuel consumption and improved overall aircraft performance.

Numerous studies and experimental evidence have demonstrated the fuel efficiency benefits of FTEFs. Case studies conducted on various aircraft configurations have shown significant reductions in fuel consumption when employing FTEFs. These studies have utilized advanced computational simulations and wind tunnel testing to assess the impact of FTEFs on aircraft performance parameters.

The European Union (EU) has long recognized the need for reducing fuel consumption and carbon emissions in the aviation industry. As part of their commitment to sustainability and environmental protection, the EU has set ambitious targets to improve the fuel efficiency of airplanes and minimize their impact on climate change.

Thus, the EU has established regulations and standards to promote the development and deployment of more fuel-efficient aircraft. For instance, the European Aviation Safety Agency (EASA) sets stringent requirements for aircraft certification, including fuel efficiency criteria. This encourages manufacturers to invest in innovative technologies and design solutions that maximize fuel economy while maintaining safety standards.

In addition to regulatory measures, the EU actively supports research and development initiatives focused

on improving aircraft fuel efficiency. Funding programs, such as Horizon 2020, provide financial support to projects aimed at developing sustainable aviation technologies. These initiatives focus on various aspects, including lightweight materials, aerodynamic improvements, and the integration of advanced propulsion systems.

Flexible trailing edge flaps represent a promising avenue for enhancing aircraft fuel efficiency, thereby serving as a potential advancement in the pursuit of sustainable aviation. Furthermore, the advancement of this technology contributes significantly to the attainment of the Sustainable Development Goals (SDGs), see in Figure 7.1. These goals encompass a comprehensive set of worldwide targets designed to tackle the most critical challenges confronting our planet and the global community.

Figure 7.1: Sustainable Development Goals. Extracted from [51].

Many of these goals are aided in their achievement through the development of this technology, including the number 9 (Innovation and infrastructure), the number 11 (sustainable cities and communities) or the number 13 (climate action).

Chapter 8

Conclusions

8.1 Project Conclusions

The current study has successfully achieved the primary objectives established at the beginning. The feasibility of designing novel structures utilizing numerical topology optimization techniques has been thoroughly investigated, resulting in positive outcomes for the development of lighter structures, specifically applied for compliant mechanisms, due to its increased importance. In particular, the methodology employed and the attained results have led to the following key findings:

The chosen programming environment for this project has proven to be instrumental at every stage, employing Object-Oriented Programming techniques to explore and embrace an enhanced programming approach. In contrast to its conventional predecessor, the function-based programming paradigm, Object-Oriented Programming offers greater reusability and dynamism, leading to optimized code development time. By using this programming methodology, a more efficient and flexible code structure has been achieved, enabling improved understanding and exploration of programming concepts.

Through an extensive review of the literature, a comprehensive understanding of the diverse range of compliant mechanism designs and their significant contributions to space exploration and technology has been achieved. By harnessing the benefits of compliant mechanisms, such as reduced mass, increased reliability, and enhanced functionality, space missions can be conducted more efficiently and effectively, paving the way for future exploration and scientific discoveries. Thus, by leveraging the knowledge and insights gained from the diverse applications of compliant mechanisms, future space missions can benefit from improved performance, increased adaptability, and enhanced mission success rates.

Moreover, through an in-depth examination of various methodologies, algorithms, and mathematical models, a comprehensive understanding of the fundamental principles and key concepts of topology optimization has been established. Throughout the section, some examples and case studies were presented to illustrate the

practical implementation and effectiveness of topology optimization in the engineering field. These examples demonstrated how topology optimization can significantly enhance the performance, efficiency, and reliability of structures, leading to weight reduction, improved material utilization, and increased functional capabilities. The obtained simulations results lead to certain conclusions. Initially, when the volume is close to 100%, the design is not a compliant mechanism (CM). However, as the simulation progresses, hinges are introduced to reverse the output displacements, resulting in a CM with a minimized negative cost function. Additionally, for designs with the same optimal volume, the resulting CM is lighter but more complex and less robust. Finally, when comparing the two design variables, it is observed that Density-based optimization struggles to achieve purely white and black results, although it may yield more accurate results for the optimal volume.

Furthermore, this section has highlighted the concept of variable geometry trailing edge flaps and their potential benefits in optimizing wing loading. Additionally, the influence of topology optimization in achieving optimal flap shapes has been emphasized. While this study did not include the development of specific code for the design, design specifications and references to existing designs have been presented as a starting point for further research.

Overall, this project has emerged as a highly significant endeavor in the pursuit of novel lightweight structures, leveraging the principles of topology optimization and compliant mechanisms. Through a comprehensive assimilation of knowledge in this domain, it is evident that this area of study currently holds paramount importance as a prominent avenue for future technological advancements, transcending the confines of the aerospace sector. The compelling implementation of these mechanisms in diverse engineering disciplines and cutting-edge technology domains underscores their indisputable relevance and positions them at the forefront of ongoing research and development endeavors.

8.2 Further lines of research

The prediction of future directions of compliant mechanisms is discussed in this section for both theory and application aspects.

Theoretically, dynamic synthesis and modeling that consider actuation position, nonlinear stiffness (including negative stiffness), beam mass, and material damping can be the next-generation directions as opposed to the current focus on static modeling. Developing the theory in stiffness-continuously-adjustable compliant mechanisms to reconfigure the dynamic characteristic of motion stage (MS) can be another interesting topic [16].

In practical applications, compliant mechanisms toward multi-material design and fabrication, programmable materials, and deployable structures (particular emphasis on compliant origami structures for DNA or space applications) should be the focus of future research [16].

Bibliography

1. SHUIB, S.; RIDZWAN, M. I. Z.; KADARMAN, A. H. Methodology of compliant mechanisms and its current developments in applications: A review. *American Journal of Applied Sciences.* 2007, vol. 4, no. 3, pp. 160–167. Available from DOI: `10.3844/ajassp.2007.160.167`.

2. GALLEGO, J. A.; HERDER, J. Synthesis methods in compliant mechanisms: An overview. In: *Volume 7: 33rd Mechanisms and Robotics Conference, Parts A and B.* 2009.

3. HOWELL, Larry L. Compliant Mechanisms. In: *Encyclopedia of Nanotechnology.* Springer Netherlands, 2016, pp. 604–611.

4. FOWLER, Robert M.; HOWELL, Larry L.; MAGLEBY, Spencer P. Compliant space mechanisms: a new frontier for compliant mechanisms. *Mechanical Sciences.* 2011, vol. 2, no. 2, pp. 205–215. Available from DOI: `10.5194/ms-2-205-2011`.

5. SHAPIRO, W.; MURRAY, F.; HOWARTH, R. *NASA Space Mechanisms Lessons Learned Study.* Cleveland, Ohio, 1995. TM, 107046. NASA Lewis Research Center.

6. FUSARO, R. L. (ed.). *NASA Space Mechanisms Handbook.* Cleveland, OH, 1999. No. 206988.

7. SELLERS, Jerry Jon. *Understanding Space – An Introduction to Astronautics.* Revised Second. McGraw Hill Custom Publishing, 2004.

8. FUSARO, Robert L. (ed.). *NASA Space Mechanisms Handbook.* Cleveland, OH: Glenn Research Center NASA/TP, 1999.

9. LEY, Wilfried; WITTMANN, Klaus; HALLMANN, Willi. *Handbook of Space Technology.* CRC Press, 2009. ISBN 978-1-60086-701-9.

10. CALOMINO, A.; LOWRY, D.; PIASCIK, B.; SCOTTI, S.; STEWART, J.; VICKERS, J. *Materials, Structures, Mechanical Systems, and Manufacturing Roadmap – Technology Area 12.* 2010. Draft Edition. NASA.

11. ADLER, M.; WRIGHT, M.; CAMPBELL, C.; CLARK, I.; ENGELUND, W.; RIVELLINI, T. *Entry, Descent, and Landing Roadmap – Technology Area 09.* 2010. draft. NASA.

12. CONLEY, P. L. (ed.). *Space Vehicle Mechanisms – Elements of Successful Design.* John Wiley & Sons, Inc., 1998.

13. GORE, B.; DIDZIULIS, S.; HILTON, M. Space Vehicle Mechanisms. *Crosslink Magazine (Aerospace Corporation).* 2006, vol. 12. Available also from: `http://www.aero.org/publications/crosslink/fall2006/03.html`.

14. *CSA Engineering* [`https://www.csaengineering.com/`]. [N.d.]. Accessed on May 18, 2023.

15. MATHEW, B. C.; BHARATPATIL, V.; ANILCHAMOLI; RAIKWAR, M.; NEGI, M. S.; SINGH, H. Compliant mechanism and origami usage in aerospace and space application. *IOP Conference Series. Earth and Environmental Science*. 2021, vol. 775, no. 1, p. 012008. Available from DOI: `10.1088/1755-1315/775/1/012008`.

16. HAO, Guo; YU, Jun; LI, Huajiang. A brief review on nonlinear modeling methods and applications of compliant mechanisms. *Frontiers of Mechanical Engineering*. 2016, vol. 11, no. 2, pp. 119–128. Available from DOI: `10.1007/s11465-016-0387-9`.

17. MA, X.; LI, T.; MA, J.; WANG, Z.; SHI, C.; ZHENG, S.; CUI, Q.; LI, X.; LIU, F.; GUO, H.; LIU, L.; WANG, Z.; LI, Y. Recent advances in space-deployable structures in China. *Engineering (Beijing, China)*. 2022, vol. 17, pp. 207–219. Available from DOI: `10.1016/j.eng.2022.04.013`.

18. LIU, T.; HAO, G. Design of deployable structures by using bistable compliant mechanisms. *Micromachines*. 2022, vol. 13, no. 5, p. 651. Available from DOI: `10.3390/mi13050651`.

19. DEWALQUE, Florence; SCHWARTZ, Cédric; DENOËL, Vincent; CROISIER, Jean-Louis; FORTHOMME, Benjamin; BRÜLS, Olivier. Experimental and numerical investigation of the nonlinear dynamics of compliant mechanisms for deployable structures. *Mechanical Systems and Signal Processing*. 2018, vol. 101, pp. 1–25. Available from DOI: `10.1016/j.ymssp.2017.08.006`.

20. KRAMER, H. J. *Myriade/AstroSat-100 (CNES Microsatellite Program)* [Eoportal.org; European Space Agency]. 2012. Available also from: `https://www.eoportal.org/satellite-missions/myriade`.

21. SICRE, J.; GIVOIS, D.; EMERIT, E. Application of Maeva hinge to Myriade microsatellites deployments needs. In: *11th European Space Mechanisms and Tribology Symposium (ESMATS) 2005*. Lucerne, Suisse: ESA/CNES, 2005.

22. DSS, D. K. Mars express. *Acta Astronautica*. 1999, vol. 45, no. 4–9, pp. 285–292. Available from DOI: `10.1016/s0094-5765(99)00145-9`.

23. MOBREM, M.; ADAMS, D. Deployment analysis of lenticular jointed antennas onboard the Mars Express spacecraft. *Journal of Spacecraft and Rockets*. 2009, vol. 46, no. 2, pp. 394–402. Available from DOI: `10.2514/1.40485`.

24. BLACK, J.T.; WHETZAL, J.A.; DEBLONK, B.J.; MASSARELLO, J.J. Deployment repeatability testing of composite tape springs for space optics applications. In: *Proceedings of the 47th AIAA/ASME/ASCE/AHS/ASC Structures, Structural Dynamics, and Materials Conference*. Newport, Rhode Island, USA, 2006.

25. COOK, A.J.; WALKER, S.J.I. Experimental research on tape spring supported space inflatable structures. *Acta Astronautica*. 2016, vol. 118, pp. 316–328.

26. JOHNSON, L.; WHORTON, M.; HEATON, A.; PINSON, R.; LAUE, G.; ADAMS, C. NanoSail-D: a solar sail demonstration mission. *Acta Astronautica*. 2011, vol. 68, pp. 571–575.

27. SICKINGER, C.; HERBECK, L. Deployment strategies, analyses and tests for the CFRP booms of a solar sail. In: *Proceedings of the European Conference on Spacecraft Structures, Materials & Mechanical Testing*. Toulouse, France, 2002.

28. YEE, J.C.; PELLEGRINO, S. Composite tube hinges. *Journal of Aerospace Engineering*. 2005, vol. 18, no. 4, pp. 224–231.

29. JEONG, Jin-Woo; YOO, Young Il; SHIN, Dong Keun; LIM, Jong Hwa; KIM, Kyung-Wook; LEE, Jae-Jun. A novel tape spring hinge mechanism for quasi-static deployment of a satellite deployable using shape memory alloy. *The Review of Scientific Instruments*. 2014, vol. 85, no. 2, p. 025001. Available from DOI: `10.1063/1.4862470`.

30. KIM, D.-Y.; CHOI, H.-S.; LIM, J. H.; KIM, K.-W.; JEONG, J. Experimental and numerical investigation of solar panels deployment with tape spring hinges having nonlinear hysteresis with friction compensation. *Applied Sciences (Basel, Switzerland)*. 2020, vol. 10, no. 21, p. 7902. Available from DOI: `10.3390/app10217902`.

31. BUDZYŃ, D.; ZARE-BEHTASH, H.; COWLEY, A.; CAMMARANO, A. Implicit lunar dust mitigation technology: Compliant mechanisms. *Acta Astronautica*. 2023, vol. 203, pp. 146–156. Available from DOI: `10.1016/j.actaastro.2022.11.042`.

32. GAIER, J.R. *The Effects of Lunar Dust on EVA Systems during the Apollo Missions*. 2007. Tech. rep., TM-2005-213610/Rev1. NASA.

33. ZIRBEL, Shannon Alisa. Compliant Mechanisms for Deployable Space Systems. 2014.

34. KOTA, S.; HETRICK, J. A.; OSBORN, R.; PAUL, D.; PENDLETON, E.; FLICK, P.; TILMANN, C. Design and application of compliant mechanisms for morphing aircraft structures. In: ANDERSON, E. H. (ed.). *Smart Structures and Materials 2003: Industrial and Commercial Applications of Smart Structures Technologies*. SPIE, 2003.

35. ZHAO, Y.; HAO, G.; CHAI, L.; TIAN, Y.; XI, F. A compliant-mechanism-based lockable prismatic joint for high-load morphing structures. *Mechanism and Machine Theory*. 2022, vol. 178, p. 105083. Available from DOI: `10.1016/j.mechmachtheory.2022.105083`.

36. ZHAO, Y.; XI, F.; TIAN, Y.; WANG, W.; LI, L. Design of a planar hyper-redundant lockable mechanism for shape morphing using a centralized actuation method. *Mechanism and Machine Theory*. 2021, vol. 165, p. 104439. Available from DOI: `10.1016/j.mechmachtheory.2021.104439`.

37. IVCHENKO, Alexander V.; SHARONOV, Nikolay; ZIATDINOV, Rinat. New conceptual design of the adaptive compliant aircraft wing frame. *Engineering Science and Technology an International Journal*. 2019, vol. 22, no. 5, pp. 1149–1154. Available from DOI: `10.1016/j.jestch.2019.10.004`.

38. MERRIAM, E. G.; JONES, J. E.; MAGLEBY, S. P.; HOWELL, L. L. Monolithic 2 DOF fully compliant space pointing mechanism. *Mechanical Sciences*. 2013, vol. 4, no. 2, pp. 381–390. Available from DOI: `10.5194/ms-4-381-2013`.

39. VIJAYAN, V.; KARTHIKEYAN, T.; KARTHIKEYAN, M.; CHELLAMUTHU, K. Passive vibration isolation by compliant mechanism using topology optimization. *The International Journal of Acoustics and Vibration*. 2014, vol. 19, no. 4. Available from DOI: `10.20855/ijav.2014.19.4359`.

40. SUN, Xiaoqing; WANG, Zhilei; YANG, Yikun. Design and experimental investigation of a novel compliant positioning stage with low-frequency vibration isolation capability. *Available online 17 June 2019*. 2019.

41. ZENG, Wen; GAO, Fei; JIANG, Hong; HUANG, Chaoliang; LIU, Jianhua; LI, Hui. Design and analysis of a compliant variable-diameter mechanism used in variable-diameter wheels for lunar rover. *Mechanism*

and Machine Theory. 2018, vol. 125, pp. 240–258. Available from DOI: `10.1016/j.mechmachtheory.2018.03.003`.

42. JAGTAP, Sachin P.; DESHMUKH, Bhushan B.; PARDESHI, Snehal. Applications of compliant mechanism in today's world – A review. *Journal of Physics. Conference Series*. 2021, vol. 1969, no. 1, p. 012013. Available from DOI: `10.1088/1742-6596/1969/1/012013`.

43. KOTA, Sridhar; LU, Kuo-Jen; KREINER, Karl; TREASE, Brian; ARENAS, Juan; GEIGER, Jeffrey. Design and application of compliant mechanisms for surgical tools. *Journal of Biomechanical Engineering*. 2005, vol. 127, no. 6, pp. 981–989. Available from DOI: `10.1115/1.2056561`.

44. FERRER, Alex. *Lessons in Topology Optimization* [Website]. 2022. Available also from: `https://sites.google.com/view/alexferrer/teaching?authuser=0`.

45. FEPPON, Florian; ALLAIRE, Grégoire; DAPOGNY, Charles. Null space gradient flows for constrained optimization with applications to shape optimization. *ESAIM. Control, Optimisation and Calculus of Variations*. 2020, vol. 26, p. 90. Available from DOI: `10.1051/cocv/2020015`.

46. NIKISHKOV, G.P. *Introduction to the Finite Element Method* [Lecture Notes]. 2001. Unpublished.

47. GARAIGORDOBIL, Asier; ANSOLA, Ricardo; VEGUERÍA, Eduardo; FERNANDEZ, Iñigo. Overhang constraint for topology optimization of self-supported compliant mechanisms considering additive manufacturing. *Computer Aided Design*. 2019, vol. 109, pp. 33–48. Available from DOI: `10.1016/j.cad.2018.12.006`.

48. AMSTUTZ, Samuel; DAPOGNY, Charles; FERRER, Anaïs. A Consistent Relaxation of Optimal Design Problems for Coupling Shape and Topological Derivatives. *Numerische Mathematik*. 2018, vol. 140, no. 1, pp. 35–94. Available from DOI: `10.1007/s00211-018-0964-4`.

49. GARAIGORDOBIL, Aitor; ANSOLA, Rafael; VEGUERÍA, Eneko; FERNANDEZ, Iñaki. Overhang constraint for topology optimization of self-supported compliant mechanisms considering additive manufacturing. *Computer Aided Design*. 2019, vol. 109, pp. 33–48. Available from DOI: `10.1016/j.cad.2018.12.006`.

50. *FlexFoil* [FlexSys]. n.d. Retrieved May 12, 2023, from `https://www.flxsys.com/flexfoil`.

51. *What is the SDG Sustainability Framework?* [Sol Vae]. n.d. Retrieved May 29, 2023, from `https://solvae.co/blogs/the-stretch/what-is-the-sdg-sustainability-framework`.

Chapter 9

Appendix

9.1 Appendix A: Constrained problems and the dual problem

In the context of constrained optimization problems, as previously discussed, it is necessary to define the Lagrangian and the dual function (which is the minimization of the Lagrangian with respect to the variable x). In this formulation, the objective is to maximize the dual function. Consequently, the primal and dual optimality conditions are expressed as the gradients of the Lagrangian with respect to x and λ, respectively.

It is particularly interesting to discuss the rationale behind maximizing the dual function. To illustrate this, let us consider the scenario where the following optimization problem is formulated:

$$\begin{aligned} \min_{x} \quad & J(x) \\ \text{s.t} \quad & h(x) = 0 \end{aligned} . \tag{9.1}$$

The optimization problem can be reformulated as

$$\min_{x} \ J(x) + \delta_c(x), \tag{9.2}$$

where δ_c is a function called indicator function which is defined as follows

$$\delta_c(x) = \begin{cases} 0 & \text{if } h(x) = 0 \\ \infty & \text{if } h(x) \neq 0 \end{cases} . \tag{9.3}$$

This is interpreted such that if the value satisfies the constraint, indicating it is a feasible value, no additional cost is incurred. However, if the value does not satisfy the constraint, an infinite value is added to the cost.

Thus, it is designed to consider only feasible solutions as valid, while penalizing infeasible solutions. This function can also be expressed using an alternative mathematical formulation:

$$\max_{\lambda} \ \lambda \, h(x). \tag{9.4}$$

It can be observed that all values are infinite (for a maximized λ) except when the constraint function $h(x)$ equals zero. Therefore, in the optimization problem, we can replace the indicator function with this alternative formulation, as

$$\min_{x} \ J(x) + \delta_c(x) = \min_{x} \ J(x) + \max_{\lambda} \ \lambda \, h(x). \tag{9.5}$$

Observe that since $J(x)$ does not depend on λ, the aforementioned formulation can also be expressed as

$$\min_{x} \max_{\lambda} \ J(x) + \lambda \, h(x) \tag{9.6}$$

where it can be observed that the expression $J(x) + \lambda \, h(x)$ represents the Lagrangian, thereby implying that the original problem formulation is equivalent to solving this problem

$$\min_{x} \max_{\lambda} \ L(x, \lambda). \tag{9.7}$$

At this juncture, it is pertinent to define the dual function $D(\lambda)$. The dual function can be perceived as a problem that is contingent upon the parameter λ, wherein for each value of λ, it entails solving a minimization problem to determine the corresponding optimal value, as

$$D(\lambda) = \min_{x} \ J(x) + \lambda \, h(x) = \min_{x} \ L(x, \lambda). \tag{9.8}$$

Now, let us consider a feasible solution $\tilde{x}$, where the constraint $h(\tilde{x})$ evaluates to zero. In this case, the Lagrangian reduces to the function $J(\tilde{x})$ alone. It can been observed that the minimum value of the Lagrangian must always be less than or equal to the Lagrangian evaluated at the feasible solution, since the latter represents a valid value and the minimization process seeks the smallest value among all possibilities, even if are not feasible. Therefore, a specific feasible value will always be equal to or greater than the minimum value obtained through the minimization process, as shown below

$$D(\lambda) = \min_{x} \ L(x, \lambda) \leq L(\tilde{x}, \lambda) = J(\tilde{x}). \tag{9.9}$$

Among all the feasible values, there exists a particular one denoted as x^* that satisfies the condition $\min_{\tilde{x}} \ J(\tilde{x})$, indicating that it is the minimum value among all feasible solutions. Thus, the following inequalities are fulfilled

$$D(\lambda) \leq J(x^*) \leq J(\tilde{x}),$$

$$\min_x \ L(x, \lambda) \leq L(x^*, \lambda) \leq L(\tilde{x}, \lambda). \tag{9.10}$$

The aim is to determine the tightest lower bound of $D(\lambda)$ among all possible values, one that is closest to $J(x^*)$. Hence, the objective is to maximize the dual function as

$$\max_\lambda \ D(\lambda) = D(\lambda^*). \tag{9.11}$$

Again, the following inequalities are fulfilled

$$D(\lambda) \leq D(\lambda^*) \leq J(x^*) \leq J(\tilde{x}),$$

$$\min_x \ L(x, \lambda) \leq \max_\lambda \min_x \ L(x, \lambda) \leq L(x^*, \lambda) \leq L(\tilde{x}, \lambda). \tag{9.12}$$

It is noteworthy that in the case of a convex problem, $D(\lambda^*)$ is equal to $J(x^*)$. Therefore, it is evident that to obtain the minimum feasible solution, the dual problem needs to be maximized. Consequently, solving the problem is equivalent to solving the following dual formulation

$$\max_\lambda \min_x \ L(x, \lambda). \tag{9.13}$$

It is of significant interest to highlight that in optimization, specifically when dealing with convex problems, utilizing the dual formulation can prove to be more advantageous compared to the primal formulation. This stems from the fact that the dual problem involves only a single unknown variable, λ, while the primal problem entails multiple unknowns. Consequently, opting for the dual formulation not only simplifies the optimization procedure but also facilitates more efficient computations. So, if there is a large number of variables but a few constrains it is better to opt for the dual formulation whereas if there is many constrains and just a few variables it should stay at the primal. Therefore, in scenarios where the number of variables is substantial while the number of constraints is relatively small, it is advisable to prefer the dual formulation. On the other hand, if the problem exhibits a significant number of constraints but only a few variables, it is more appropriate to adhere to the primal formulation. By considering the nature of the problem in terms of variable-constraint proportions, the selection between the primal and dual formulations can be optimized to enhance computational efficiency and problem-solving effectiveness.

9.2 Appendix B: Result obtained for a gripping mechanism using MMA optimizer

The MMA optimizer is particularly suitable for problems with a large number of design variables and constraints. It is an iterative method that seeks to find the optimal solution by updating the design variables based on a set of subproblems.

At each iteration, the MMA optimizer updates the design variables by solving a set of subproblems. These subproblems involve minimizing a penalized objective function subject to the constraints, where the penalties are adjusted based on the previous iteration's design variables.

One of the advantages of the MMA optimizer is its ability to handle both inequality and equality constraints. It employs a constraint aggregation technique that converts inequality constraints into a series of penalty functions, allowing for a unified treatment of all constraints.

While the integration of the MMA optimizer was not initially included within the scope of this thesis, a series of supplementary simulations were conducted to explore alternative perspectives of the optimization problem. These simulations aimed not only to expedite the solution process compared to the computationally-intensive Null Space optimizer but also to gain insights into the obtained results from different vantage points.

Thus, Figure 9.1 shows the result of a gripping mechanism simulation for a volume fraction of 0.3 and for the design variable Density.
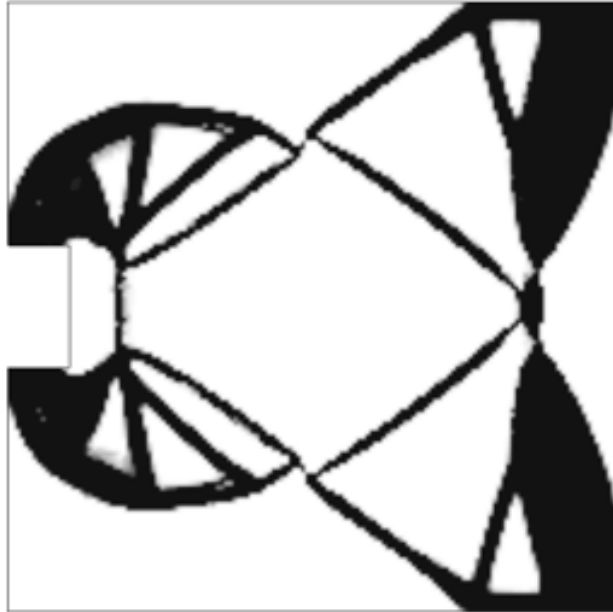

Figure 9.1: Result of the simulation using MMA optimizer.

It is evident that the solution obtained using the MMA optimizer exhibits notable similarities with the results obtained using the Null Space optimizer. However, a distinct characteristic of the MMA optimizer is the presence of significantly more holes and hinges in the obtained solution.